Author/s:
Neto, LAB;Narsilio, GA;Makasis, N

Title:
Analytical interpretation and numerical analysis of multiple energy pile thermal response tests

Date:
2023-05

Citation:
Neto, L. A. B., Narsilio, G. A. & Makasis, N. (2023). Analytical interpretation and numerical analysis of multiple energy pile thermal response tests. Computers and Geotechnics, 157, https://doi.org/10.1016/j.compgeo.2023.105314.

Persistent Link:
https://hdl.handle.net/11343/332480

Analytical interpretation and numerical analysis of multiple energy pile thermal response tests

Author 1
Luis A. Bandeira Neto, MSc (Geotech), CEng
Department of Infrastructure Engineering, The University of Melbourne, Parkville, Australia
ORCID: 0000-0002-4314-2637

Author 2
Guillermo A. Narsilio✉, PhD, MSc (Math), MSc (CE), CEng
Department of Infrastructure Engineering, The University of Melbourne, Parkville, Australia
ORCID: 0000-0003-1219-5661

Author 3
Nikolas Makasis, PhD, MSc (CS), ME (CIEV), CEng
Department of Engineering, University of Cambridge, Cambridge, England
Department of Infrastructure Engineering, The University of Melbourne, Parkville, Australia
ORCID: 0000-0002-6678-1239

Full contact details of corresponding author
Guillermo A. Narsilio, Deputy Head of Department (Research) and Professor
Engineering Block B 205, Department of Infrastructure Engineering, The University of Melbourne, Parkville, VIC 3010, Australia
Email: narsilio@unimelb.edu.au, Phone: +61 (3) 8344 4659, Fax: +61 (3) 8344 4616

Abstract:

Thermal response tests (TRT) are an essential in situ test for the sizing of ground source heat pump systems. Its application on energy piles is becoming an established practice, involving key differences in relation to testing boreholes. Recently, group TRTs emerged as an alternative to testing single short energy pile elements. This work assesses the execution and interpretation of those tests through different analytical heat transfer models implemented in a unit-response calculation methodology. To assess the suitability of the method, a comprehensive parametric analysis using a validated numerical model is undertaken, considering different energy pile sizes, thermal properties for both concrete and soil and group pile arrangements. The analytical methodology is validated against experimental and numerical results, and then tested to interpret the numerically simulated TRTs using a curve fitting algorithm. The broad parametric investigation and the evaluation of the capacity of different analytical methods on modelling each scenario provide directions to execute and interpret group TRTs. The soil effective thermal conductivity and energy pile thermal resistance are obtained with less than 5% precision error for most scenarios and less than 10% considering all scenarios. These results can be further improved with specific individual G-functions for the pile elements, that can be implemented on the proposed methodology.

Keywords
Energy Piles; Thermal Response Tests; Analytical Models; Numerical Modelling

Highlights

- Thermal inteference influences the results of multi-energy pile TRT.
- The intensity of thermal interference between piles depends on the soil and pile geometry.

- The interpretation of closely spaced multi-pile TRT must consider thermal interactions.
- An analytical method for interpreting any multi-pile TRT is presented.

List of Notations

$C_{p,c}$	concrete specific heat capacity
$C_{p,f}$	fluid specific heat capacity
$C_{p,g}$	ground specific heat capacity
$\mathbf{D}$	thermal resistance matrix
$\mathbf{d}$	thermal disturbance history vector
Err	relative error (%)
Fo	Fourier Number
$\mathbf{G}$	step G-function matrix
G	G-function
G_g	Pile ground G-function
G_c	Pile concrete G-function
$G_{i,i}$	Pile individual response G-function
$G_{i,j}$	Pile to pile interference G-function
H	Total heat exchanger length
h	individual pile/borehole length
$\mathbf{h_t}$	vector of length of individual piles in a pile group
$\mathbf{L}$	pipe-to-pipe connection matrix
m	slope of the linear relation between average carrier fluid temperature and $\log_n(t)$
$\dot{m}$	mass fluid flow rate
n_{piles}	number of energy piles in series

P	estimated values (from the methodology proposed)
Q	total thermal power (W)
q	thermal power transfer rate (W/m)
q_{rate}	circulating fluid flow rate
$\mathbf{Q_t}$	thermal power transfer vector containing the total heat exchange by each GHE
$\mathbf{q_t}$	vector of 1 x n_{piles} individual piles thermal power transfer rates
R_b	Pile thermal resistance
$r_{b,}$	pile radius
r	radial coordinate
s	pile spacing
T_{avg}	system average fluid temperature
$T_{farfield}$	undisturbed ground temperature
T_{in}	system inlet fluid temperature
T_{out}	system outlet fluid temperature
T_0	undisturbed ground temperature
V	"real" value (from the FE model).
α_g	ground thermal diffusivity
γ	Euler constant
λ_c	concrete thermal conductivity
λ_f	thermal conductivity of fluid
λ_g	effective ground thermal conductivity
ρ_c	density of concrete
ρ_f	density of fluid
ρ_g	density of ground
z	vertical coordinate (depth)

1 Introduction

Ground source heat pump systems (GSHP) are a renewable energy alternative for heating and cooling buildings that makes use of shallow geothermal energy through heat exchangers embedded in the ground. The employment of geostructures to also act as heat exchangers can reduce the implementation cost of GSHP systems significantly (Lu & Narsilio, 2019), thus expand their applicability. Energy piles are the most researched energy structure, however implementation of this technology at a larger scale is inhibited by the lack of proper serviceable design methods (Loveridge et al., 2020; Narsilio & Aye, 2018). The similarities (e.g., cylindrical slender shape) to the extensively employed borehole heat exchangers (BHE) initially propelled energy piles research with its established applicable models. However, pile structural design and lower aspect ratio (AR = length / diameter) introduce differences to thermal design from BHE practice (Brandl, 2006; Makasis et al., 2018; Loveridge et al., 2014).

The Thermal response test (TRT) is the leading in-situ test tool for ground thermal characterisation and thus BHE design. The test consists of injecting (or extracting) thermal power at a constant rate by circulating a heated fluid (e.g. water) in the heat exchanger's pipes while measuring the fluid inlet and outlet temperatures. TRTs were first implemented on boreholes (Austin III, 1998; EklÖF & Gehlin, 1996; Mogensen, 1983) and later applied on energy piles (Bouazza et al., 2013; Colls et al., 2012; Murphy et al., 2014; Wood et al., 2010), while nowadays their use has expanded to other energy structures as well (Motamedi et al., 2021; Zhong et al., 2022). The outcomes from this test are the effective ground thermal conductivity (λ_g) and the BHE thermal resistance (R_b), the latter being a reciprocal to thermal conductivity, capturing the effective thermal response within BHE (Beier & Smith, 2002; Loveridge & Powrie, 2014a). In practice, the main TRT analytical interpretation tool used is based on the log-linear approximation of the infinite line source model (ILSM) (Carslaw & Jaeger, 1959), popular due to the ease of computation and low computational requirements. Zhang et al. (2019) compared different analytical methods on interpreting a TRT executed in a borehole and its impact on design, concluding that ILSM is precise enough when interpreting TRTs. The ILSM log-linear approximation requires that the early-stage data of the test, typically equivalent to the heat exchanger heating stage (i.e., transient phase), to be discarded. The duration of the transient phase depends on the

BHE diameter and the soil conditions (Gehlin, 2002; Hellstrom, 1992), ranging from a few hours for boreholes to up to a few days for large piles. The requirement of significantly longer TRT for energy piles jeopardizes its application, since longer tests are more expensive and more exposed to power fluctuations and eventual faults (Loveridge et al., 2014).

There are several examples of problems related to TRT execution on piles, and some respective studies addressing them. Bouazza et al. (2013) and Morais et al. (2020) presented experimental large energy pile TRT cases where over 100 hours of test had to be discarded for proper test interpretation and yet the results present a significant variability. Franco et al. (2016) used numerical models to evaluate the sensitivity of interpretation of TRTs using the simplified form of the ILSM to certain parameters, concluding that the thermal conductivity of both soil and concrete, pipe spacing, and pile diameter may induce more significant influence on the test results. In an attempt to shorten energy piles TRTs duration, Loveridge et al. (2014) tested the applicability of transient Pile G-functions (Loveridge & Powrie, 2013) on the test interpretation. The Pile G-functions interpretation resulted in similar parameter values to the ones obtained using the ILSM for typical TRT duration, however the Pile G-functions needed a shorter test duration. Even though the pile tested by Loveridge et al. (2014) is relatively small (0.3 metres diameter), Jensen-Page et al. (2019) arrived to similar conclusions regarding the pile G-functions and the ILSM analysing an energy pile with 0.6 m diameter. Moreover, Jensen-Page et al. (2019) concluded that FE models are still more reliable overall.

However, to the best of the authors' knowledge no work to date assessed the interpretation of TRT tests for energy pile groups, with only a handful of exploratory articles available in the literature. As per Katsura et al. (2009), a group of energy piles connected in series can be modelled as a single-long heat exchanger, therefore the test could be interpreted as such. Loveridge et al. (2015) analysed a TRT executed in a group of three energy piles, concluding that the consideration of an equivalent single long BHE can be used for interpretation. Bandeira Neto et al. (2023) compared the suitability of TRT between a test executed in a single short energy screw pile and another executed in a group of eight equivalent piles, concluding the group test was a better approach. The authors interpreted the TRTs using FE models and ILSM approximation, assuming the piles in the group formed a single equivalent

borehole as per the literature. The parameters obtained analytically were consistent with the FE model results. Analysis of the FE model outputs confirmed that there was no significant pile-to-pile thermal interference occurring, which may eventually happen in a group test.

This work evaluates the thermal interferences that may occur in group TRTs and assesses what is the impact in the group test execution and interpretation. A validated FE model is used to simulate hundreds of TRTs in both boreholes and pile groups, observing how the arrangement, geometry and thermal parameters affect the carrier fluid temperature. The largely used assumption that piles in series behave as a single-long heat exchanger is tested in the analysis of the model's outputs. An analytical method able to simulate the thermal behaviour of energy pile groups during a TRT is presented and validated against the FE models and a full scale TRT executed in a group of eight energy piles. This analytical method is then used to interpret the group TRTs, aiming to obtain λ_g and R_b with at least similar precision that traditional TRT interpretation methods achieve for single heat exchangers.

2 Analytical heat transfer models

This section presents a brief review of the main analytical models used on BHEs and energy pile practice that are considered in this work.

2.1 Single heat exchanger models

Most analytical heat transfer models used in BHE practice are named after the main assumptions involved. For instance, the **ILSM** assumes that the BHE behaves as an infinite linear source of heat, while the Infinite Cylindrical Source Model (**ICSM**) assumes an infinite cylindrical shape and the finite linear source model (**FLSM**) in turn assumes a finite linear shape. The equations and details on these traditional analytical models are presented in Appendix A, however they can all be simplified as presented by (Eq. (1))

$$T(t) = T_0 + qR_b + qG \tag{1}$$

where G stands for G-function (Eskilson, 1987), that corresponds to the ground thermal response. In each one of these analytical methods there is a corresponding G-function (Li & Lai, 2015) which are indicated in Appendix A. These models consider R_b as a constant, representing the steady state thermal

resistance of the BHE, which can be obtained from different methods (Marcotte & Pasquier, 2008). However, during the transient phase, R_b is not constant (Bidarmaghz, 2014). This assumption is suitable for boreholes, however for energy piles with large diameters, which have a longer transient phase, it is less appropriate. Loveridge and Powrie (2013) developed specific energy Pile G-functions, generated from the results of several FE models metres (Eq. (2)):

$$T(t) = T_0 + qG_cR_b + qG_g \quad (2)$$

where G_c is named as the Pile concrete G-function, and G_g is the Pile ground G-function. The purpose of G_c is to model the transient phase; its value varies from zero to one, building up the R_b value until the steady state is reached. Because of the problem complexity, Loveridge and Powrie (2013) could not define a single equation for either G_c or G_g. The Pile G-function equations are defined by characteristics of the problem. The functions are limited by upper and lower bound conditions (PGUB and PGLB, respectively) that correspond to different early stages behaviour, and pile AR from 15 up to 50, which characterise the late stage.

2.2 Thermal interferences between piles

Usual GSHP design configurations with multiple BHEs consist of an evenly spaced grid, hence thermal interactions are rather uniform. Eskilson (1987) also developed BHE group G-functions that consider evenly spaced borehole grids by calculating FLSM solutions for multiple distances and considering the spatial superposition of effects. For clarity, the schematic in Figure 1 presents two energy piles connected in series rejecting thermal power to the ground. The thermal power injected in Pile 1 heats up both Pile 1 and Pile 2. The thermal response of Pile 1, to determine its average carrier fluid temperature (T_{avg}), is given by Eq. (3).

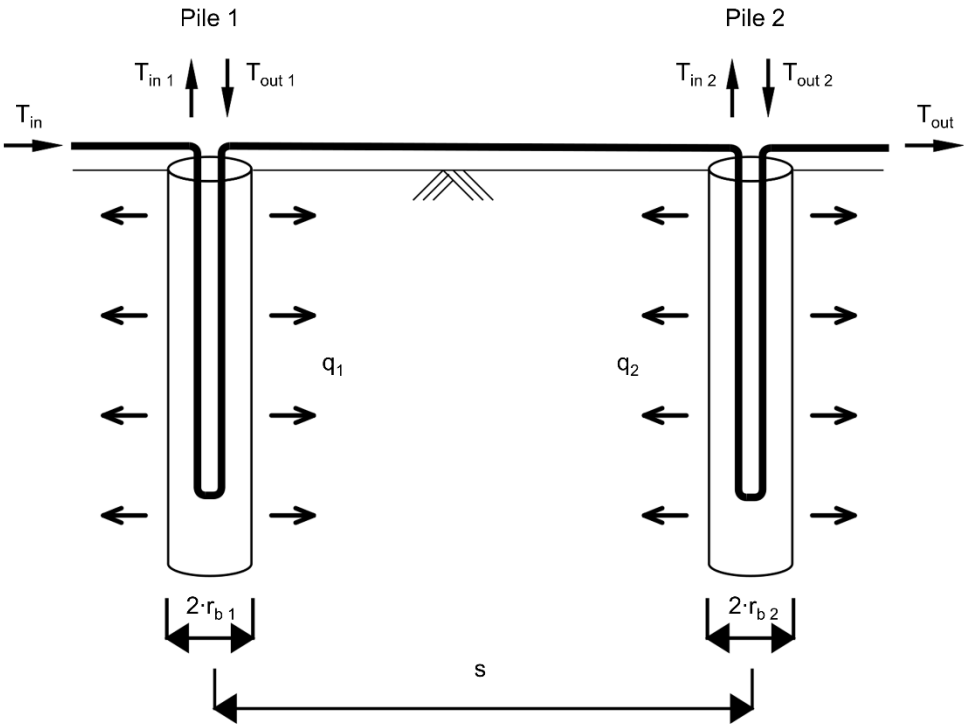

Figure 1 Representation of two energy piles connected in series.

$$T_1(t) = T_0 + q_1 R_{b,1} + q_1 G_{1,1} + q_2 G_{1,2} \quad (3)$$

where $G_{1,1}$ is the Pile 1 individual thermal response G-function, and $G_{1,2}$ is the Pile 2 interference on Pile 1 ground G-function. While $G_{1,1}$ is solved for the distance r_{b1}, $G_{1,2}$ is calculated considering pile spacing distance *s* to compute the thermal interference. To calculate the outlet fluid temperature leaving Pile 2 (T_{out}), the sum of both thermal resistance components, both individual pile responses, and the thermal interference from each pile over its counterpart must be considered (hence, a superposition of effects). Consequently, the combination of the existing G-functions forms the respective BHE group G-function as done by Eskilson (1987). However, energy piles distribution is usually irregular, and pile geometries vary due to the structural design, denoting multiple r_b and s values. So instead of developing several group G-functions, Loveridge and Powrie (2014b) presents a methodology to determine G-functions for any pile configuration using FE models. However, this method does not account for the case when piles are connected in series.

The energy pile spatial distribution and pipe-to-pipe connection configuration affect the amount of thermal power transferred by each pile over time. When energy piles or boreholes are connected in series, the first pile in the sequence exchanges more thermal power since its inlet temperature will be

more extreme in comparison to the following one. In addition, piles exposed to less thermal interference can exchange more thermal power over time, as they receive less of it from neighbouring piles. Consequently, the individual q_i values of each pile over time are unknown. Marcotte and Pasquier (2014) propose an algorithm to solve the fluid temperature and individual borehole heat transfer on borehole fields of any geometry and pipe-to-pipe connection using the superposition of FLSM solutions. The solution of the linear system presented bellow (Eq. (4)) provides both parameters:

$$\begin{bmatrix} \boldsymbol{G} + \boldsymbol{D} + \boldsymbol{L} & 1 \\ 1^T & 0 \end{bmatrix} \begin{bmatrix} \boldsymbol{Q_t} \\ -(T_{in} - T_0) \end{bmatrix} = \begin{bmatrix} -\boldsymbol{d} \\ Q \end{bmatrix} \quad (4)$$

where **G** is the step G-function matrix, that contains solved FLSM functions for all existing r_b and s values , **D** is the thermal resistance matrix, **L** is the pipe-to-pipe connection matrix, $\mathbf{Q_t}$ is the thermal power transfer vector containing the thermal power absorbed in each BHE, T_{in} is the system inlet fluid temperature and **d** is the thermal disturbance history vector, that contains the thermal response of each pile before the time step to be solved. More details on the methodology can be found in (Marcotte & Pasquier, 2014). This approach allows fast and precise analytical calculation of complex BHE systems and was validated against FE models; however, it has not been tested on energy piles yet. This work modifies the original algorithm to provide the average fluid temperature instead of the inlet and uses other G-functions besides the one from the FLSM to model and interpret TRTs on energy pile groups.

3 Methodology

This work uses a validated FE numerical model to undertake a parametric analysis of single and group TRTs. A total of 468 scenarios are simulated, providing data and insight into the thermal response of energy pile groups in comparison to equivalent single heat exchangers. The parametric analysis shows the impact of thermal interferences between piles in a group TRT result. An analytical tool based on the knowledge presented in section 2.2 and validated against both the numerical results presented in this work and a full-scale energy pile group TRT from the literature. The tool is then used to interpret λ_g and R_b values of all simulated group tests, examining the errors involved while aiming for feasibly shorter test duration, outlining the applicability of each interpretation method in practice. Details of this overview and general approach are included in this section.

3.1 FEM model's parametric analysis

FE models with a single borehole and multiple energy piles are used to simulate TRTs. All models consider the heat exchangers embedded within a single soil material layer. The soil is considered as homogeneous and isotropic, and only heat conduction is considered within the soil (i.e., no groundwater flow) while both convection and conduction are considered in the pipes. Groundwater flow may affect the TRT result interpretation (Li et al., 2022; Magraner et al., 2021). However, in practice the groundwater flow effect is commonly considered within the resulting effective thermal conductivity (Franco & Conti, 2020) since the most popular analytical models do not account for groundwater flow. Groundwater flow is not considered in the numerical models for this work and is expected to be investigated in future work. Continuity and energy balance governing equations are numerically solved through implementation in the FEM package COMSOL Multiphysics (COMSOL, 2021). The pipes and the circulating water are modelled as 1D elements, coupled to the 3D pile and soil elements by the pipe wall temperature. No thermomechanical effects are considered for simplicity. Further information on the governing equations involved can be found in Appendix B and (Bidarmaghz, 2014; Makasis, 2019) and several (real and synthetic) cases of validation for this methodology can be found in the literature (Bidarmaghz et al. 2016; Jensen-Page et al., 2019; Makasis et al., 2018), including one against a group of eight energy screw piles connected in series (Bandeira Neto et al., 2023).

Four model geometries are built, including a single borehole and two, four and eight energy piles. To simplify the comparison between scenarios with different number of piles, the total heat exchanger length is kept constant to 100 metres and all piles are connected in series. Therefore, the single BHE has 100 metres depth while in the group of eight piles each one has 12.5 metres depth, assuming the pipe connections between piles are insulated, therefore not contributing towards these values. The meshing of the different geometries results in a total element number range varying from 300,000 to up to 460,000 tetrahedral elements, depending on the generated domain since the size varies according to the various pile spacings modelled sequentially (Figure 2 and Table 1). The boundary conditions are thermal insulation on the top and constant temperature ($T_{farfield}$) on the bottom and lateral boundaries, which are at least 10 metres distant to the closest pile (Figure 2). The same average thermal power rate

of 50 W/m is used as input (i.e., both BHE and pile groups are subjected to 5kW heating) to calculate the inlet fluid temperature in each time step (Appendix B). The simulation time is 14 days, ensuring that all tests would at least exceed the duration threshold of Fo = 5. The simulation time step adopted is 15 minutes for the first 24 hours (where more changes are seen in temperature) and 2 hours for the remainder. A single high-density-polyethylene pipe (HDPE) U-loop is inserted in each pile, with the pipes positioned 5 cm from the pile wall, meaning that pipe spacing varies with the pile diameter. Besides the number of piles, different values for the effective ground thermal conductivity λ_g, the concrete thermal conductivity λ_c, the pile radius r_b, and the pile spacing s are considered in the analysis. All other parameters are kept equal to the ones used in model validation (Bandeira Neto et al., 2023). The parameters values are presented in Table 1, comprising a total of 432 simulated scenarios with multiple piles and another 32 of a single borehole.

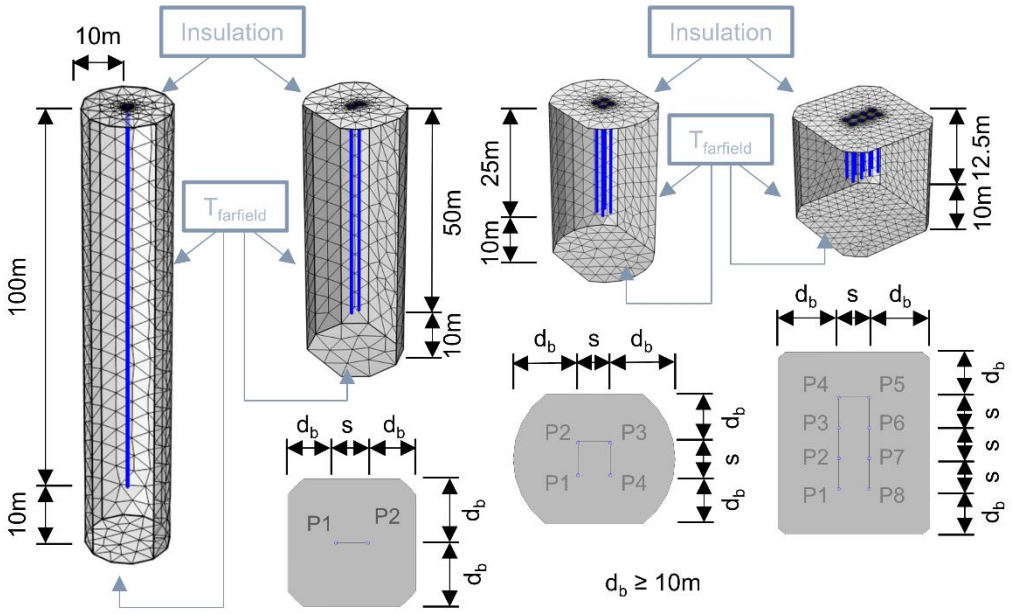

Figure 2 Geometries of the models with one, two, four and eight piles (not to scale) considering Thermal insulation (1) and Fairfield temperature (2) as top and sides boundary conditions, respectively.

Table 1 Parameters considered in the model parametric analysis

Parameter	Value(s)	Unit	Description
λ_g	1, 2, 3 and 4	W/(m·K)	Effective ground thermal conductivity
λ_c	1, 2 and 3	W/(m·K)	Concrete thermal conductivity
r_b	75, 150 and 250	mm	Energy pile radius
s	1, 2, 5 and 10	m	Spacing between energy piles

n_{piles}	1, 2, 4 and 8	-	Number of energy piles
ρ_g	2000	kg/m^3	Density of ground
$C_{p,g}$	1000	J/(kg·K)	Specific heat capacity of ground
ρ_c	2250	kg/m^3	Density of concrete
$C_{p,c}$	890	J/(kg·K)	Specific heat capacity of the concrete
λ_f	0.58	W/(mK)	Fluid thermal conductivity
ρ_f	998	kg/m^3	Fluid density
$C_{p,f}$	4185	J/(kg·K)	Fluid specific heat capacity
$T_{farfield}$	18	°C	Undisturbed ground temperature
q_{rate}	25	L/min	Circulating fluid flow rate

From the model results, the relative thermal efficiency of each pile group is evaluated as the percentage of total thermal power retained TP_{ret} by each group of piles in comparison to its equivalent 100 m single borehole (same thermal properties and BHE radius). The calculation of TP_{ret} is done by comparing the fluid temperature increase between the group of piles and the respective equivalent boreholes, which represent the total energy exchanged, since for the TRTs the thermal power used is the same. Larger thermal power retained means lower relative heat transfer efficiency, defined as:

$$TP_{ret} = \frac{T_{f,group}(t = 14\ days) - T_{farfield}}{T_{f,bore}(t = 14\ days) - T_{farfield}} - 1 \quad (5)$$

where TP_{ret} is the thermal power percentage that the pile group fails to reject in the soil due to thermal interference, $T_{f,group}$ and $T_{f,bore}$ are the fluid temperatures of the pile group and boreholes scenarios, respectively, which have the same r_b, λ_g and λ_g.

In addition to the parametric analysis, the numerical models are used to validate and evaluate an analytical methodology for group TRT interpretation, described in sections 3.3 and 3.4.

3.2 Proposed thermal interference methodology

The methodology presented herein is based on the work of Marcotte and Pasquier (2014), with a few modifications made to allow the estimation of TRT parameters and consider different analytical models for the calculation of the G-functions. The matrix **D** (Eq. (4)) is removed from the general equation and included in the matrix **G** calculation, given the existence of the concrete G-function G_c in the pile G-

functions. In addition, here the problem is solved in terms of thermal power transfer rate q (W/m) instead of total thermal power Q (W). The vector $\mathbf{Q_t}$ from Eq. (4) can be written as ($\mathbf{q_t}$·$\mathbf{h_t}$), where $\mathbf{q_t}$ is a 1 x n_{piles} vector of the individual piles thermal power transfer rates for the moment in time considered in the calculation, and $\mathbf{h_t}$ is a vector of the same size composed by the length of each pile. Therefore, the total thermal power exchanged in the system can be described as $Q(t) = H \cdot q(t) = \left(\sum_1^{n_{piles}} q_i(t) \cdot hi\right)$. As in the case studied herein all piles have the same length or depth ($H = h \cdot n_{piles}$) the thermal power transfer rate of the system becomes $q(t) = \frac{\left(\sum_1^{n_{piles}} q_i(t)\right)}{n_{piles}}$. Lastly, to work in terms of average fluid temperature $T_{avg} = (T_{in} - T_{out})/2$, the term T_{in} in Eq. (4) is replaced by T_{avg}, which requires the thermal interference matrix **L** to be modified, following the assumption from Eq. (6). The system is presented on Eq. (7):

$$T_{avg} = T_{in} - \frac{Q}{2\dot{m}C_{p,f}} \tag{6}$$

$$\begin{bmatrix} \boldsymbol{G} + \boldsymbol{L} & 1 \\ 1^T & 0 \end{bmatrix} \begin{bmatrix} (\boldsymbol{q_t} \cdot \boldsymbol{h_t}) \\ -\left(T_{avg} - T_0\right) \end{bmatrix} = \begin{bmatrix} -\boldsymbol{d} \\ q \cdot n_{piles} \end{bmatrix} \tag{7}$$

where $\dot{m}$ is the mass fluid flow rate and $C_{p,f}$ is the fluid specific heat capacity. The matrix **G** has a size of n_{piles} x n_{piles} and has the following shape:

$$\boldsymbol{G} = \begin{bmatrix} G_{1,1} & G_{1,2} & \cdots & G_{1,j-1} & G_{1,j} \\ G_{2,1} & G_{2,2} & \cdots & G_{2,j-1} & G_{2,j} \\ \vdots & \cdots & \ddots & \cdots & \vdots \\ G_{i-1,1} & G_{i-1,2} & \cdots & G_{i-1,j-1} & G_{i-1,j} \\ G_{i,1} & G_{i,2} & \cdots & G_{i,j-1} & G_{i,j} \end{bmatrix} \tag{8}$$

where $G_{i,j}$ is the G-function calculated for the thermal response caused by pile *j* over pile *I* in a time t_{step}. For instance, when *i* = *j*, $G_{i,i}$ corresponds to the individual pile thermal response (e.g., like $G_{1,1}$ in the RHS of Equation (3)), while when $i \neq j$, $G_{i,j}$ corresponds to the pile-to-pile thermal interference from pile *j* in the thermal response of pile *i* (e.g., like $G_{1,2}$ in the RHS of Eq. (3)). The individual pile response functions are solved considering the respective R_b value of each pile, while the thermal interference function consider R_b = 0. In this work, other analytical models besides the FLSM (used by Marcotte

and Pasquier (2014)) are used for the calculation of the G-functions. The connection matrix **L** has the following shape, considering all piles connected in series:

$$\boldsymbol{L} = \begin{bmatrix} 0 & \frac{-1}{2\dot{m}C_{p,f}} & \cdots & \frac{-1}{2\dot{m}C_{p,f}} & \frac{-1}{2\dot{m}C_{p,f}} \\ \frac{1}{2\dot{m}C_{p,f}} & 0 & \cdots & \frac{-1}{2\dot{m}C_{p,f}} & \frac{-1}{2\dot{m}C_{p,f}} \\ \vdots & \cdots & \ddots & \cdots & \vdots \\ \frac{1}{2\dot{m}C_{p,f}} & \frac{1}{2\dot{m}C_{p,f}} & \cdots & 0 & \frac{-1}{2\dot{m}C_{p,f}} \\ \frac{1}{2\dot{m}C_{p,f}} & \frac{1}{2\dot{m}C_{p,f}} & \cdots & \frac{1}{2\dot{m}C_{p,f}} & 0 \end{bmatrix} \quad (9)$$

The Matrix **L** can be modified to solve parallel-only or mixed connections systems by changing the corresponding $L_{i,j}$ and $L_{j,i}$ values to zero when piles *i* and *j* are connected in parallel instead. This is not required in this paper, as all cases simulated have piles connected in series only. This methodology assumes that no heat loss occurs on the surface pipes ($T_{out,i} = T_{in,i+1}$).

Finally, the vector **d** is the thermal response history vector, where each element is the thermal response of each pile in the system calculated prior to the current time-step (starting from **d** = 0). The calculation of the thermal response history is complex and time-consuming since it requires considering the temporal superposition of effects for each pile. However, it can be obtained faster through the convolution product of $\mathbf{(q_i * f_i)(t)}$, where $q_i(t)$ is the thermal power transfer rate (W/m) step function, f_i is the analytical model thermal response function (both corresponding to the same pile *i*) and t is the time passed before the current calculation step. The convolution product can be efficiently computed using Fast Fourier Transform (FFT) (Lamarche & Beauchamp, 2007b; Pasquier & Marcotte, 2013). The unknowns of the linear system are the average fluid temperature T_{avg} and each pile thermal power transfer rate q_i.

The methodology is validated by simulating the same 432 group tests from the FE models. In addition, a full-scale TRT test in a group of eight energy screw piles is simulated analytically and the results compared to the experimental measurements. The root mean squared error (RMSE) of both the mean fluid temperature and the thermal power rejected per pile are analysed to validate the methodology

247 before employing Eq. (7) with curve fitting to interpret TRT results, described in the following section.
248 Different analytical models (ILSM, ICSM, FLSM and both PGUB and PGLB Pile G-functions) are
249 used to calculate the matrix **G** and the thermal history vector **d** to evaluate which analytical models
250 provide the best fit.

251 3.3 Group TRT analytical interpretation

252 In evaluating the suitability of the analytical models for TRT analysis, two different approaches are
253 used for comparison (Figure 3). In the first approach, λ_g and R_b are obtained for each one of the 468
254 scenarios using the common TRT interpretation based on the ILSM log-linear regression (Appendix A
255 – Eqs. A.2 and A.4). This method, hereafter named *Traditional approach*, does not account for eventual
256 thermal interferences between neighbour piles, since it assumes each case (pile group or individual pile)
257 as an equivalent single 100 m borehole heat exchanger.

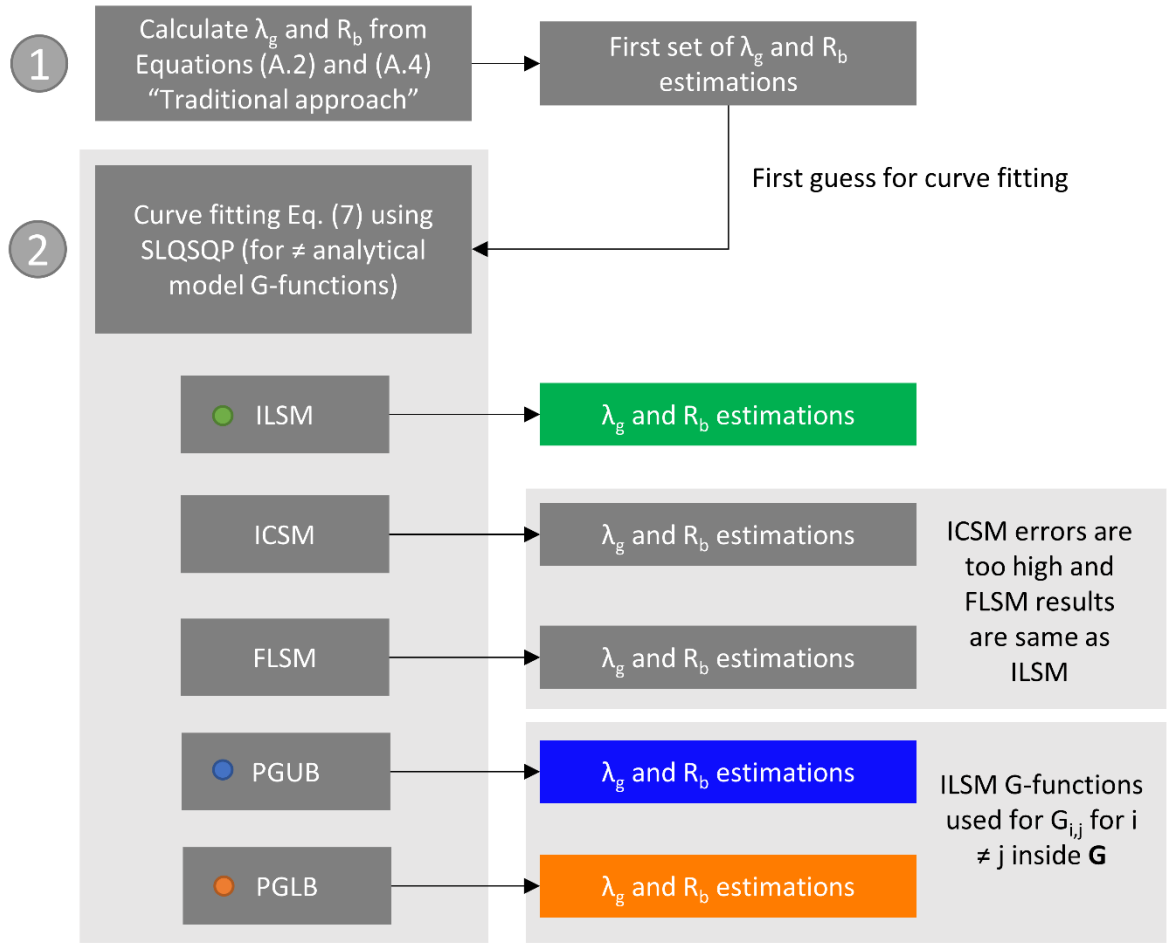

Figure 3. Process adopted to obtain each one of the analytical TRT estimations of λ_g and R_b: (1) The "Traditional approach" which does not account for pile-to-pile thermal interference, and (2) the "Thermal Interference approach", which is applied considering G-functions from all five models.

In a second approach, hereafter named *Thermal Interference approach*, the values obtained from the Traditional approach serve as first guesses for a curve fitting parameter estimation process using the Sequential Least Squares Programming SLSQP algorithm to estimate the correspondent parameters that minimises the T_{avg} difference between the analytical methodology that do account for piles' thermal interferences and the one virtually generated for each of the FE models. The SLSQP algorithm allows the use of bound constrains for the estimations, as recommended by Li and Lai (2012b) for TRT interpretation using curve fitting. The analytical calculations are undertaken using the methodology described in section 3.2 on all scenarios with multiple piles; populating the **G** matrix with G-functions from the different analytical models presented in section 2[1]. The G-functions are solved for the distance

[1] All five analytical models in Section 2 were tested in the Thermal Interference approach. Following what was observed in section 4.2, the ILSM, PGUB and PGLB models perform the best in predicting average fluid temperature, thus Section 4.3 presents the new group TRT interpretation methods based on these three.

r_b when calculating the pile individual response (Section 2.1, $G_{i,j}$ for $i=j$) and the pile spacing s when calculating the pile-to-pile thermal interference (Section 2.2, $G_{i,j}$ for $i \neq j$). It is important to notice that in the work of Loveridge and Powrie (2013) the Pile G-functions are reasonably approximated to zero below certain low *Fo* values (i.e., early on in time). However, for the implementation of these G-functions in the methodology presented here, the small thermal changes that may happen in a t_{step} cannot be ignored in the **G** matrix calculation. To implement the Pile G-functions in **G**, the t_{step} value adopted is adjusted to the lowest time where the Pile G-function is different from zero. Because this results in a large t_{step} values for larger pile to pile distances, the Pile G-functions cannot be utilized for calculation of the off-diagonal elements of **G** (the pile-to-pile thermal interference, $G_{i,j}$ for $i \neq j$). Instead, the pile-to-pile G-functions from ILSM is used for $G_{i,j}$ for $i \neq j$ in **G**. However, for the calculation of the diagonal elements of **G** (the individual pile thermal response, $G_{i,j}$ for $i = j$) both PGUB and PGLB are used, each one on its respective interpretation. Both PGUB and PGLB equations adopted in this work considers the pipes are positioned at the edge of the pile (Loveridge & Powrie, 2013).

Each interpretation provides one value of λ_g and one of R_b, which are compared to the values from the corresponding FE model (taken as the "true" values) to evaluate accuracy. While λ_g is a FE model input, the numerical R_b value needs to be calculated using Eq. (10). Since the value of R_b varies with time, the average value over time after $Fo = 5$ is chosen as a representative value for each case.

$$R_b = \frac{1}{q}\left(\overline{T_f} - \overline{T_b}\right) \tag{10}$$

where $\overline{T_f}$ and $\overline{T_b}$ are the integral mean temperature values from the circulating fluid and the pile/borehole wall, respectively.

The TRT interpretation methods (Figure 3) are repeated for different time windows of the test when interpreting the data (i.e., when fitting the analytical results to the "true" numerical ones), as the analytical models may have a better fit for certain heat transfer phases. Time windows ≥ 24 hours were generated using pair of values shown in Table 2 (e.g., time window between 2 and 24 hrs; 2-36 hrs; 96-144; 120-144 hrs; 364-336 hrs; etc.).

Table 2 Starting and ending times pair of values used in generating various time windows for the TRT interpretation analysis.

Time values (hours)									
2	6	12	18	24	36	48	60	72	96
120	144	168	192	216	240	264	288	312	336

In total, over four hundred thousand TRT interpretations are undertaken, considering different test scenarios (combinations of values in Table 1), analytical methods (ILSM, FLSM, ICSM, PGUB and PGLB, besides the Traditional approach), and time windows (176 pair-wise combinations from Table 2). The quality of the estimations of λ_g and R_b in each interpretation is evaluated using the percentual relative error *Err* between the estimated parameter value *P* (from the analytical methodology introduced here) and the "true" value *V* (used in the FE simulation). Negative *Err* values indicate underestimation while positive values indicate overestimation:

$$Err = \frac{P - V}{V} \cdot 100 \tag{11}$$

The parameter estimation using the different configurations and models has been implemented using the Python programming language and the SciPy package (Jones, Oliphant, Peterson, & others, 2001). To execute this large number of analyses, parallel processing has been adopted using High Performance Computing facilities at The University of Melbourne.

4 Results and discussion

4.1 Test simulations analysis

By comparing the fluid temperature of the models with multiple piles against their borehole equivalent, it is possible to evaluate the loss of thermal power transfer efficiency of the pile groups caused by the thermal interactions. For each combination of λ_g, λ_c and r_b values, the rise of the fluid temperature is compared between the single BHE model and the equivalent models with two, four and eight piles. Figure 4 presents the boxplot of this metric, described by thermal power retained TP_{ret} defined in Eq. (5), shown for each group of piles, all parameter combinations and the different pile spacing in each tested group. For larger spacing values (5 and 10 metres) TP_{ret} is insignificant, which indicates that the pile group behaves similar to a single BHE. However, the difference increases for cases with smaller

spacing, where higher values of n_{piles} further increase the fluid temperature difference, due to more elements interacting.

Figure 5 presents a further breakdown for all scenarios with pile spacing s = 1 metre, where the TP_{ret} values are the highest in Figure 4. It can be observed that the thermal interference is larger for higher values of λ_g, λ_c and r_b. While the first two parameters are related to the speed at which the thermal power travels within the respective material, the increasing thermal interference with the increase in r_b is related to the resulting increase in the pipe spacing. In larger piles, the pipes are further away from the centre of the cross section and closer to other energy piles. In comparison to a BHE of an equivalent total length, the group of piles can exchange on average around 4.5%, 10.3% and 14.3% less thermal power, for 2, 4, and 8 pile groups respectively, with a maximum of 72.6% in extreme cases. The relative efficiency of the group increases in scenarios with sufficient pile spacing, and benefits from lower values of λ_g, λ_c and r_b.

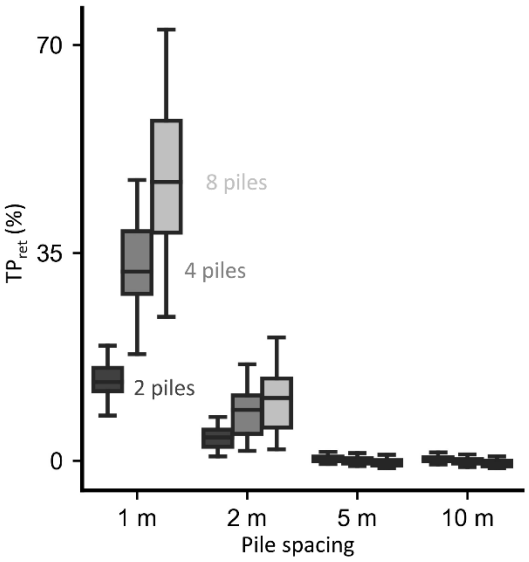

Figure 4. Thermal power retained by the groups with 2, 4 and 8 piles in comparison to their equivalent single borehole scenario, grouped by their pile to pile spacing.

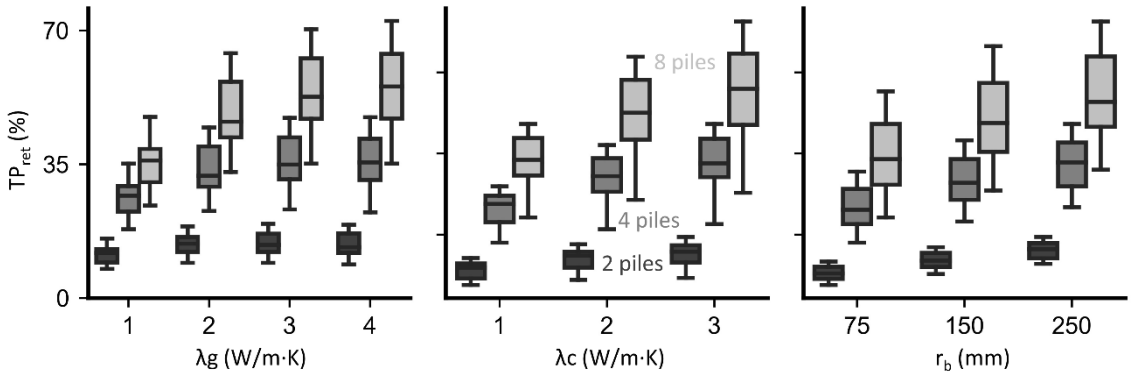

Figure 5 Thermal power retained by the groups with 2, 4 and 8 piles with pile spacing of 1 metre in comparison to their equivalent single borehole scenario. Grouped by influence of λ_g , λ_c and r_b.

Figure 6 pictures the undergoing thermal interferences during the TRT simulations with two piles 1 metre apart (Figure 6). Two combinations of λ_g, λ_c and r_b are selected, which enable the highest (λ_g = (4 W/(m·K)), λ_c = (3 W/(m·K)) and r_b = 25 cm) and lowest (λ_g = (1 W/(m·K)), λ_c = (1 W/(m·K)) and r_b = 7.5 cm) thermal power flow. Importantly, these two combinations also represent the highest and lowest values of TP_{ret}, and therefore the lowest and highest relative thermal efficiency, respectively (i.e., when a high heat flow is enabled through the parameters, thermal interference increases, hence relative thermal efficiency decreases). The undergoing thermal interference is clear in both scenarios in Figure 6, occurring faster in the scenario with highest thermal power flow, while in the models with 5 m or higher spacing the 20 °C contours (blue circles) never overlap. However, the fact that the fluid temperature is relatively low shows that the thermal power is also driven away faster due to the higher λ_g, which reduces the degree at which the soil is heating the piles nearby. While for lower thermal power flow the temperatures are more extreme, the difference of the multiple pile geometries and the single borehole is smaller than with higher thermal power flow where piles are close enough (Figure 5). Therefore, the relative efficiency of scenarios with high thermal power flow is lower.

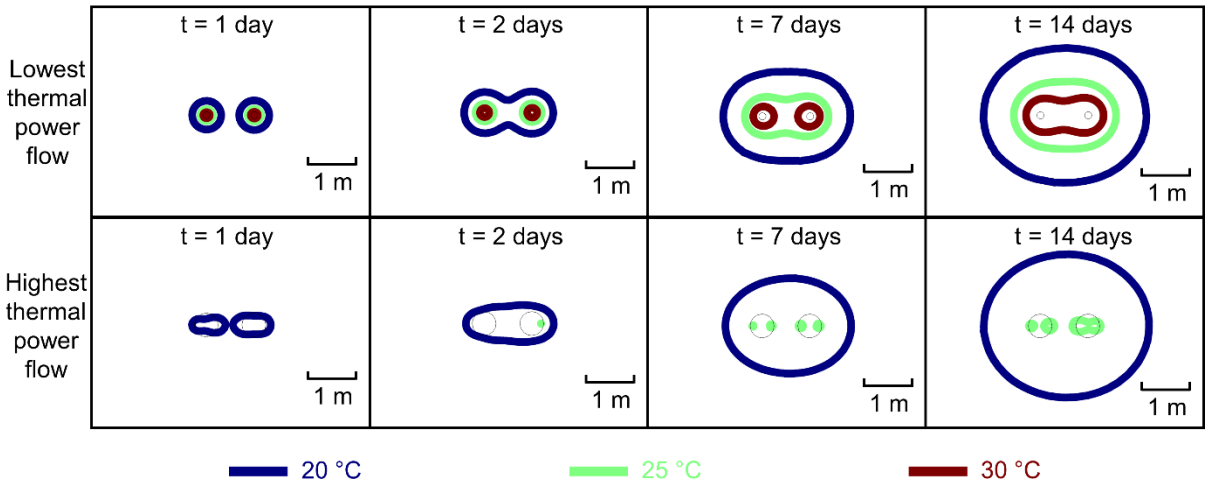

Figure 6 Temperature contour plot of different times from the models with lowest and highest thermal power flow, considering scenarios with 2 piles 1 m apart.

Figure 7 presents the percentage of the total thermal power that each pile rejects to the ground over time on two of the models with eight piles connected in series. The model with highest thermal power flow (based in the description from the previous paragraph) presents a greater percentage difference between piles, while the lowest thermal power flow model shows relatively small differences between piles. The reason behind that is the higher individual pile efficiency on rejecting thermal power due to the better thermal properties, leaving less energy in the circulating water for the next pile, regardless of the pile spacing. A steady state condition can be observed for s = 10 metres. Nevertheless, when s = 1 metre, no steady state is achieved within the simulated 14 day TRT time. Moreover, the thermal interference in the short spacing affects the thermal power rejected per pile accordingly to its position. The piles in the corners (P1, P4, P5 and P8, recall Figure 2) have lower interference from neighbouring piles. Consequently, the temperature rise for these occurs slower, and they tend to reject more thermal power with time. Piles near the centre reach higher temperatures faster becoming less efficient at rejecting heat. Proper analytical TRT interpretation of group tests require an analytical method capable of capturing the thermal interferences and individual pile thermal loads.

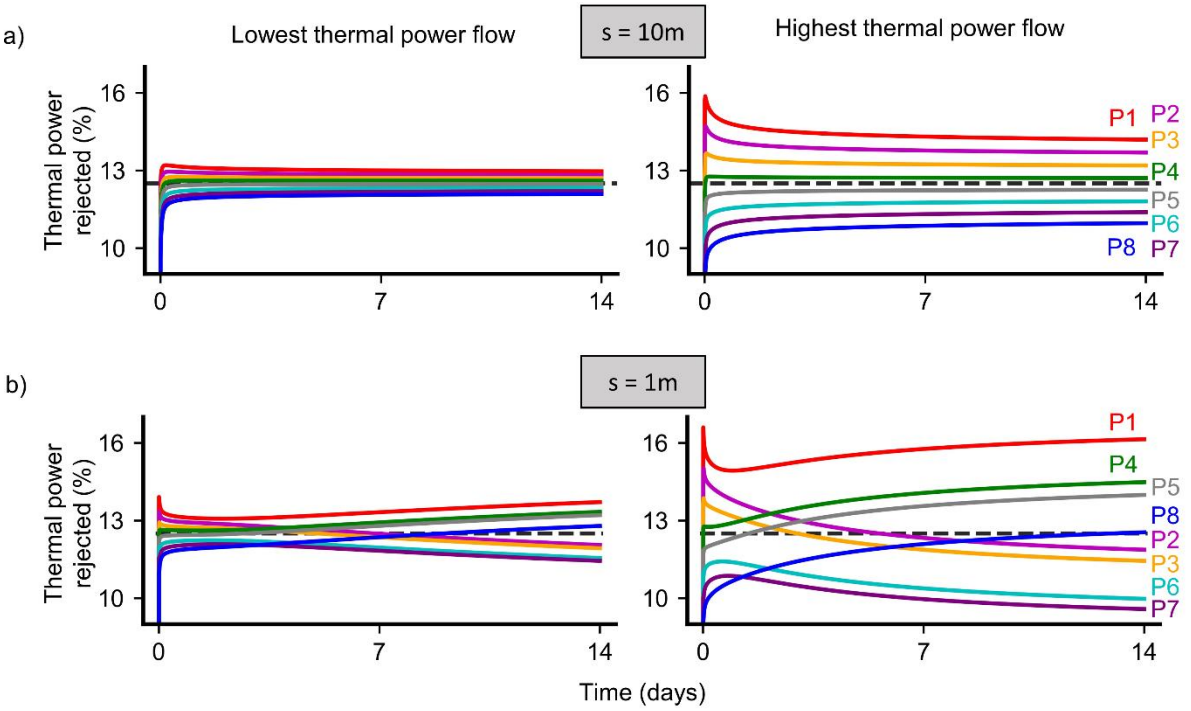

Figure 7 Percentage of thermal power rejected per pile in the group of eight piles, with lowest and highest thermal power flow thermal parameters combination, and 10 m (a) and 1 m (b) spacing. The dashed line represents the average percentage of thermal power rejected per pile for the eight pile system.

4.2 Thermal interference tool

4.2.1 Numerical verification

To verify the suitability of Eq. (7) to model TRTs on energy pile groups, the 432 tests with multiple energy piles simulated with numerical models are reproduced analytically, using the methodology described in section 3.2. The analytical methods do not use λ_c as a direct input, yet it is used to compute the thermal resistance. The thermal resistance R_b can be obtained analytically using a variety of methods (Jensen-Page et al., 2019; Loveridge & Powrie, 2014a). However, the R_b value used in each analytical calculation in this section is obtained from the numerical FE models using Eq. (10), this would render the "true" R_b value or "best in class", avoiding any errors arising from analytical approximations.

Figure 8 presents the RMSE values of each one of the analytical models used to calculate the G-functions in Eq. (8). The thermal interference methodology can replicate the difference of thermal power rejected per pile (Figure 7), given the low RMSE values observed in Figure 8b), where no variation can be noticed between the different analytical models. Observing the mean fluid temperature, the RMSE values of the ICSM stand out (up to 4 °C) while all other models' results have a similar range with values of RMSE under 1 °C for most cases. These results agree with existing literature, where

similar performance of the ICSM compared to other analytical methods was observed for single heat exchangers (Jensen-Page et al., 2019; Man et al., 2010; Yu et al., 2013). The ILSM and FLSM models presented very similar RMSE values. The reasoning for this is that that the main difference between the two models, the consideration of a finite heat source, is mostly important in later phases of heat rejection, when the axial heat transfer becomes dominant (Li & Lai, 2012a; Philippe et al., 2009). Even for the short piles with 12.5 metres length, the 14-day period seems insufficient to reach that heat transfer phase.

Breaking down the results from Figure 8 by the different parameters in the analysis enables observing where each model performs the best or worst in Figure 9. The thermal conductivity of the ground, λ_g, seems to affect both ICSM and PGLB results, with higher conductivity values resulting in lower errors. For the ILSM and FLSM models, only the λ_c value (and thus R_b) seems to impact the performance of the simulations, with lower λ_c values / higher R_b values resulting in a higher error values for these models. Since none of the models used, other than the Pile G-functions, consider the transient behaviour of R_b and assume a constant value, it is expected that these models would perform worse where R_b value is higher. The Upper boundary Pile G-functions (PGUB) also presents a higher RMSE for lower λ_c because their usage is recommended for piles with high thermal conductivity. The Lower Boundary Pile G-functions (PGLB) would be the recommended one for lower λ_c. However, Loveridge and Powrie (2013) indicate that for $Fo \leq 0.25$, PGLB should be approximated to zero. As explained in section 3.3, the time step has to be increased for the implementation of these functions in the stepwise algorithm. $Fo = 0.25$ translates into almost 9 hours for the models for $\lambda_g = 1$ W/(m·K) and $r_b = 0.25$ m. This justifies the higher RMSE values observed for low λ_g and high r_b values for the PGLB. For the PGUB function, the thermal response is approximated to zero when $Fo \leq 0.01$, which translates into less than 1 hour for all scenarios. The smaller time step size adopted in the analytical modelling with the PGUB justifies its best overall performance in comparison to PGLB. The fact that the pile spacing value impact is negligible indicates that the functions utilised are suitable to model both the piles individual response and the pile-to-pile thermal interference.

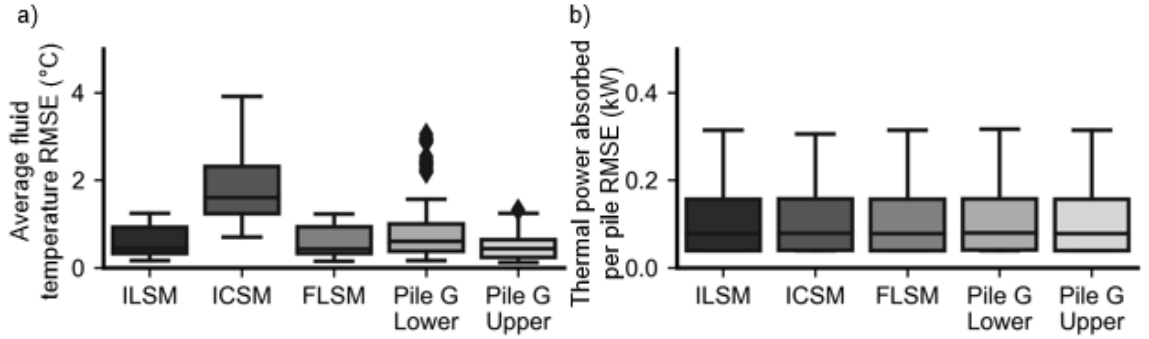

Figure 8. Mean Fluid temperatures (a) and thermal power absorbed per pile (b) RMSE values (analytical versus numerical) from 432 group TRTs, using the listed analytical models inside the thermal interference algorithm.

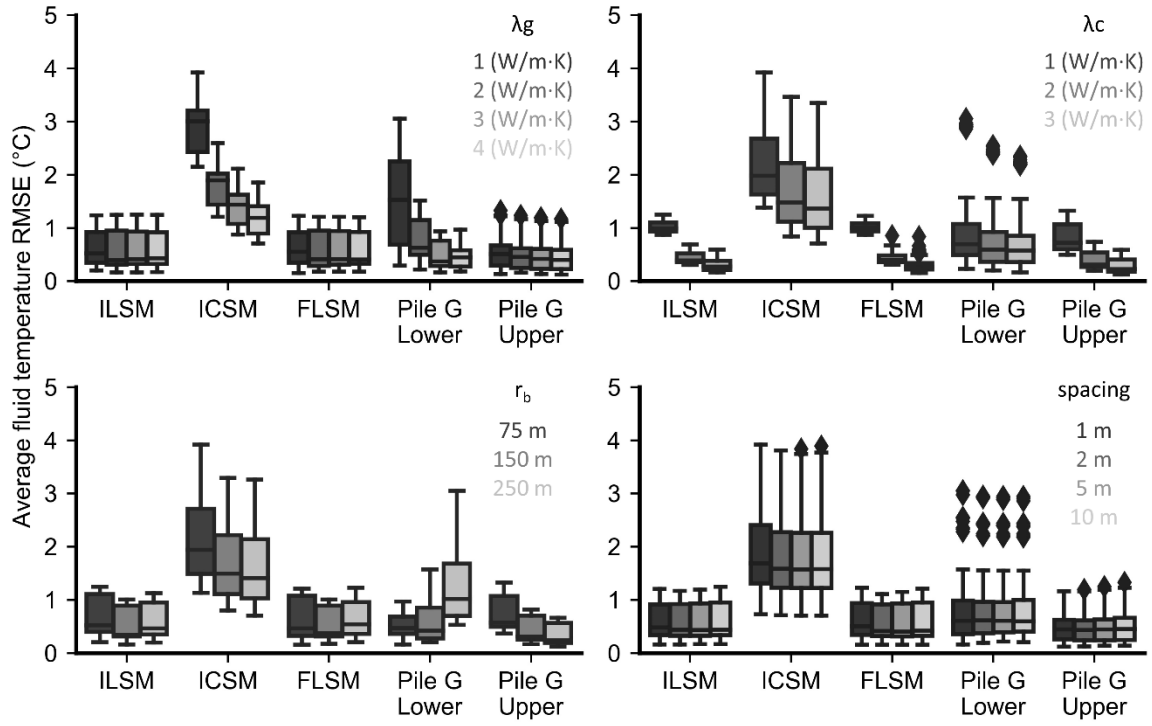

Figure 9. Mean fluid temperature RMSE values (analytical versus numerical) of 432 group TRTs, using the listed analytical models inside the thermal interference algorithm, grouped by influence of λ_g , λ_c, r_b and pile spacing.

To perform an even more detailed analysis, a few scenarios from Figure 9 are selected. Figure 10 presents the results of the analytical and numerical FE simulations of geometries with eight piles and pile spacing of 1 metre and 10 metres. The lowest and highest thermal power flow thermal parameters combinations are chosen again as defined in section 4.1. In all figures the grey dashed line marks the time where *Fo* = 5 on each model. The scenario with 10 metres spacing (solid lines) is compared against the ILSM analytical solution, showing some errors in the early stages of the test (before *Fo* = 5 in Figure 10a) and earlier in b), and a very good agreement for the latter stages. The model with 1 metre spacing (dashed lines) is compared against the ILSM, PGLB and PGUB analytical solutions. The results show

that after a certain time the ILSM fluid temperatures rise faster than the FE models. The PGLB results match best with the lowest thermal power flow scenario, while the PGUB agrees with the highest thermal power flow scenario. Regarding the widely used time threshold of *Fo* = 5, the beginning of agreement of analytical results to the FE models happen around the threshold for Figure 10a) and earlier than the threshold for Figure 10b), for both scenarios, the Pile G-functions match the numerical results earlier in time then ILSM. These observations reinforce the suitability of *Fo* = 5 as the minimum threshold for TRT analysis when using the ILSM. However, a high λ_c value speed up the convergence of the numerical and analytical model results.

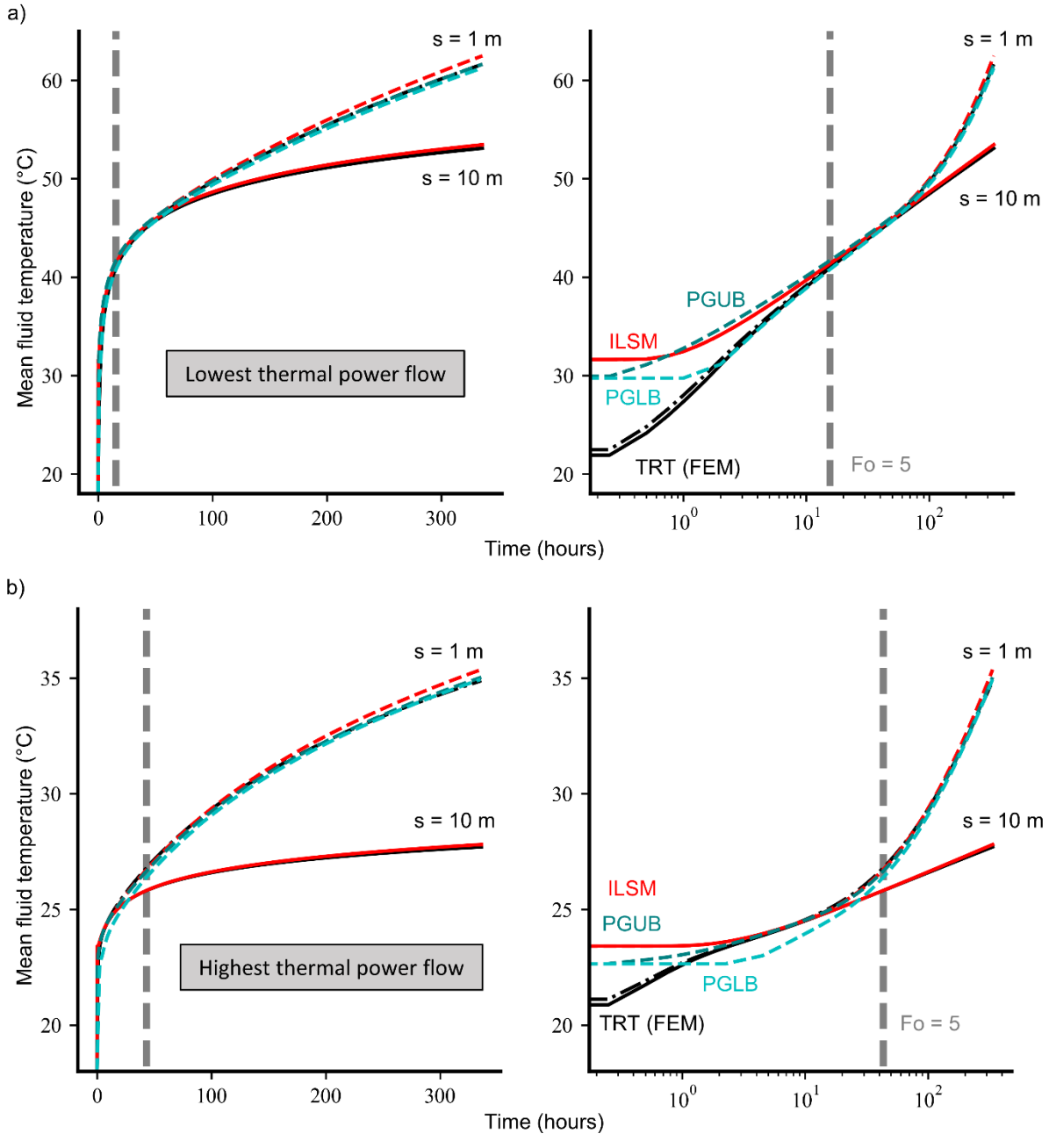

Figure 10 Mean fluid temperature over time in normal (left) and in semi-log (right) plots of the lowest (a – λ_g = 1 W/(m·K); λ_c = 1 W/(m·K); D = 0.15 m) and highest (b – λ_g = 4 (W/m·K); λ_c = 3 (W/m·K); D = 0.5 m) thermal power transfer models with eight piles spaced 1 and 10 metres apart (dashed and solid lines respectively).

4.2.2 Experimental verification

To verify the applicability of the analytical methodology from section 3.2 beyond the FE simulations, a full scale TRT executed in a group of eight energy screw piles with average pile spacing of ~3m is simulated using the analytical thermal interference approach, and the results are compared to the experimental measurements. The details of the thermal response test can be found in Bandeira Neto et al. (2023). Given the small diameter of the piles (114 mm) and the relatively low ground thermal conductivity (1.5 W/(m·K)), the ILSM is chosen to generate the G-functions to calculate the G-matrix (Eq. (8)) for both individual pile responses and pile-to-pile interference for the eight tested piles, following the learnings within these sections and considering Figure 9.

The comparison between analytical and experimental data is shown in Figure 11. Plot a) presents the measured carrier fluid inlet and outlet temperatures over time and the corresponding analytically calculated values, while plot b) presents the comparison between both. The difference observed in Figure 11b) is due to an overestimation of the fluid temperature by the analytical calculation at the earliest stages of the test due to not modelling the thermal resistance transient phase. Since the transient phase represents a short period of the test (i.e., small pile diameter), the impact of not considering it in this case is negligible and can barely be noticed in Figure 11a). For larger piles, however, where the transient phase is important, the Pile G-functions may provide a more suitable result. The suitability of different analytical models' G-functions for simulating different scenarios may depend on the group TRT geometry and arrangement and result in distinct interpretation strategies.

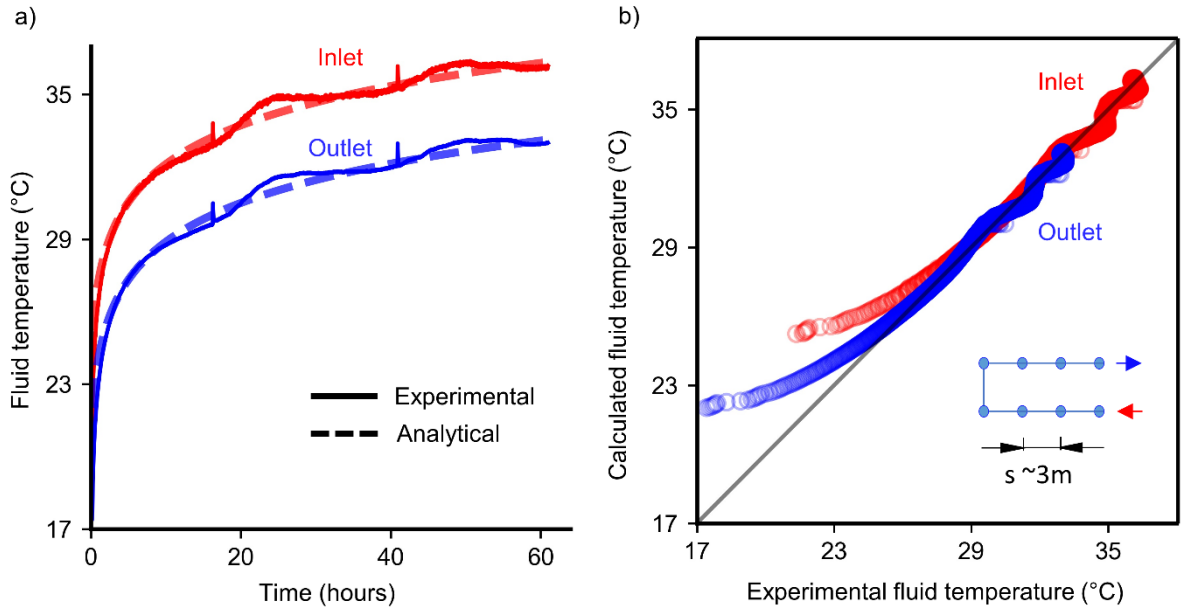

Figure 11. Experimental and analytical fluid temperature values plots over time (a) and 1-on-1 (b) of a TRT executed in a group of eight energy screw piles connected in series (data from (Bandeira Neto et al., 2023)).

4.3 Group TRT interpretation

Following the procedure described in section 3.3, the temperatures obtained using numerical simulated TRTs are used in the Traditional approach (which does not account for thermal interactions) to obtain estimations of λ_g and R_b. Figure 12a) presents the error of these estimations (computed analytical value versus 'real' numerical input parameter) considering the test time window between $Fo = 5$ and the end of each simulation. Even though this consideration results in an uncommonly long test duration for most scenarios (typical TRT duration is around 50 hours after $Fo = 5$ (Franco & Conti, 2020)), the estimation error using the Traditional approach on single BHEs is lower for longer tests. Consequently, a similar outcome would be expected for group TRTs assuming a similar behaviour to an equivalent long BHE. Unsurprisingly, the error values from Figure 12a) are higher for scenarios with lower spacing and more piles, where the pile-to-pile thermal interference is greater. On scenarios with piles spacing ≤ 2 m, the Traditional approach underestimates λ_g (negative error values) and overestimates R_b (positive error values) because there is high pile-to-pile thermal interference which is ignored by the Traditional approach. Therefore, the Traditional approach interprets the fluid temperature increase resulting from the thermal interference between piles as unrealistically low thermal conductivity and high thermal resistance. When pile spacing is large enough (5 m or higher), the estimation error range is very similar to the scenarios with just one borehole, suggesting that the Traditional approach can be used to interpret

group TRTs the same way as individual BHE as long as there is no significant pile-to-pile thermal interference.

For comparison, the newly proposed analytical Thermal Interference approach is used to interpret the same test group pile scenarios. Figure 12b) presents the estimation error results of the Thermal Interference approach using the ILSM G-functions to populate the **G** matrix and the thermal history **d** vector considering the same time window from Figure 12a) (Fo = 5 until the end). The ILSM G-functions are selected for consistency with the Traditional approach (explained in Appendix A). In comparison to Figure 12a), the estimation errors decrease significantly for the closely spaced pile scenarios, while for scenarios with spacing $s \geq 5$ metres the error values remain similar (Figure 12b). Therefore, the Thermal Interference approach improves analytical parameter estimation of scenarios where thermal interference is significant. However, there is still an influence of the number of piles and their spacing on the λ_g and R_b estimations errors, as larger errors are observed for smaller pile spacing and larger number of piles in Figure 12b). This indicates that, even though the Thermal Interaction approach reduced the estimation errors, the degree of thermal interference still affects parameter estimation accuracy. Since there is a deviation of the multi-pile analytical simulation results (s = 1 m and using the ILSM G-functions) from the FE models after a certain time (roughly between 100 and 200 hours – Figure 10 – section 4.2.1), it is possible that the estimation error could be reduced by selecting a different interpretation time window.

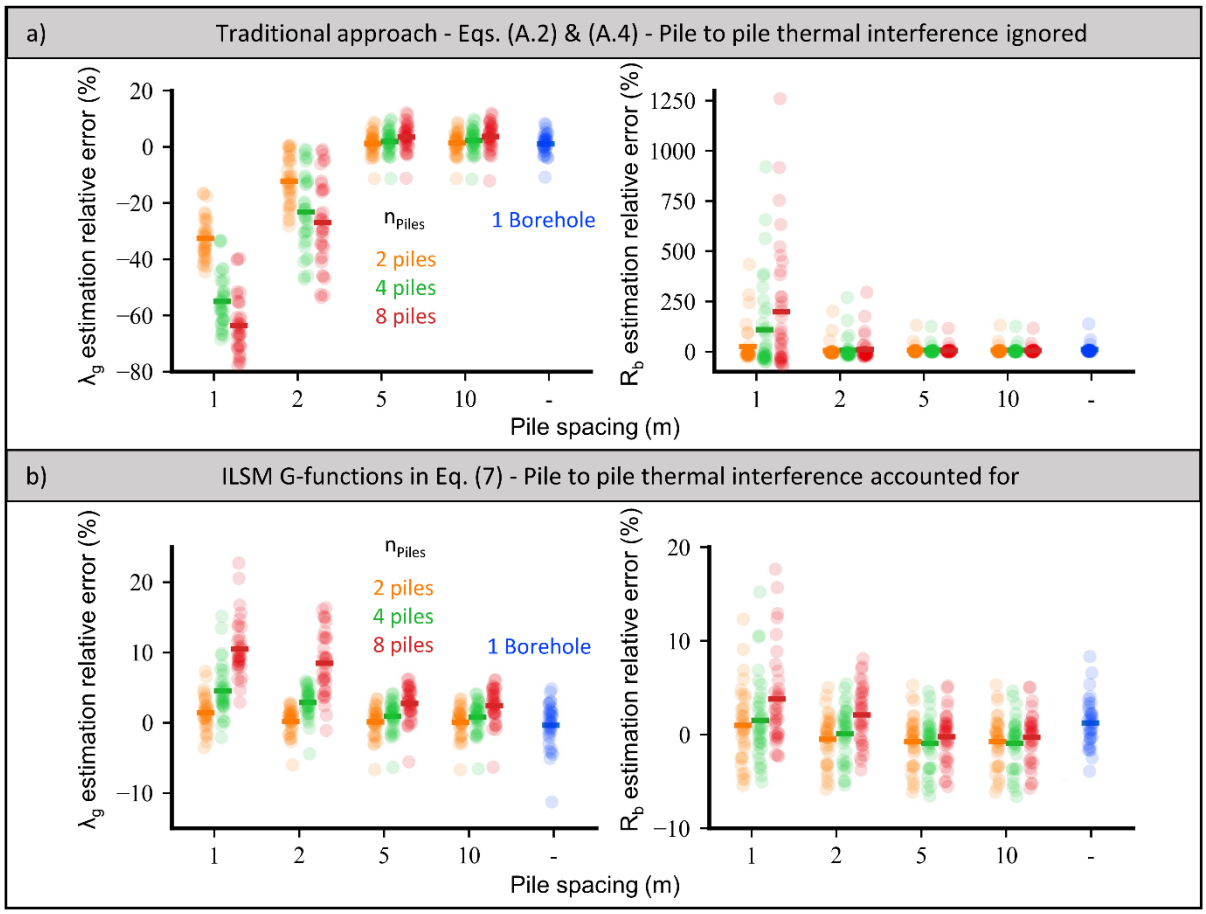

Figure 12. Estimation relative error of λ_g and R_b using the Traditional approach (a) and using the Thermal Interference approach (b) [note the change of y-axis scale between (a) and (b)].

To investigate this, the estimations errors of all interpretation windows described in section 3.3 (Table 2) are split in three groups, enabling the analysis of the time window selection impact on the estimation error: 2-96 hours, 48-168 hours, and 168-336 hours, hereafter labelled as "early", "mid" and "late" test periods respectively. Figure 13 presents the estimation errors obtained when interpreting the TRTs with the Thermal Interference approach (with ILSM G-functions) for the mentioned time windows. To analyse the influence of both λ_g and λ_c values simultaneously, the λ_g / λ_c parameter ratio is presented on the x axis. Overall, the estimation errors of both λ_g and R_b are larger when late testing periods are analysed (Figure 13c), contrariwise to what is observed when the Traditional approach is used to interpret single borehole TRTs. This is related to the observed difference on fluid temperature obtained when simulating the same TRT using the analytical thermal interference methodology (with ILSM G-functions) and the numerical models on later test times for close-spaced scenarios (red and black dashed lines in the left side of Figure 10a) and b). This implies that the ILSM G-functions overestimate the

fluid temperature on the long-term thermal interferences' calculation, therefore are less suitable to interpret TRTs using late time windows. Moreover, the early time window estimation errors are overall higher than the mid time windows errors (Figure 13a) and b), respectively), likely due to the known unsuitability of the ILSM for modelling early TRT stages (which originated the adoption of $Fo = 5$ as a threshold for traditional single BHE TRT interpretation). During earlier time windows, of the values of r_b and λ_c influence the estimation of λ_g. The λ_g values is overpredicted when λ_c is greater than λ_g (lower λ_g/λ_c ratio) and underpredicted when λ_c is lower than λ_g (greater λ_g/λ_c ratio) as a result of the influence of λ_c. This effect is more pronounced for larger piles, where the representative volume of λ_c is larger, hence the value of λ_c affects the estimation accuracy of λ_g if the test duration is not long enough.

The estimation of λ_g using mid-range time windows present the lowest error values and lowest variance (Figure 13b), while for the estimations of R_b the same occurs in the early time windows. This happens because the relative sensitivity of the ILSM to λ_g increases with time, while it remains constant for R_b (Franco et al., 2016; S. Zeng, Yan, & Yang, 2022); since the thermal interferance methodology is a superposition of ILSM G-functions, the relation between λ_g and R_b sensitivities is similar. Therefore, when interpreting group TRTs using the Thermal Interaction approach with the ILSM G-functions, the interpretation of the early test times provides a better estimation of R_b while mid-range time windows provide a better estimation of λ_g.

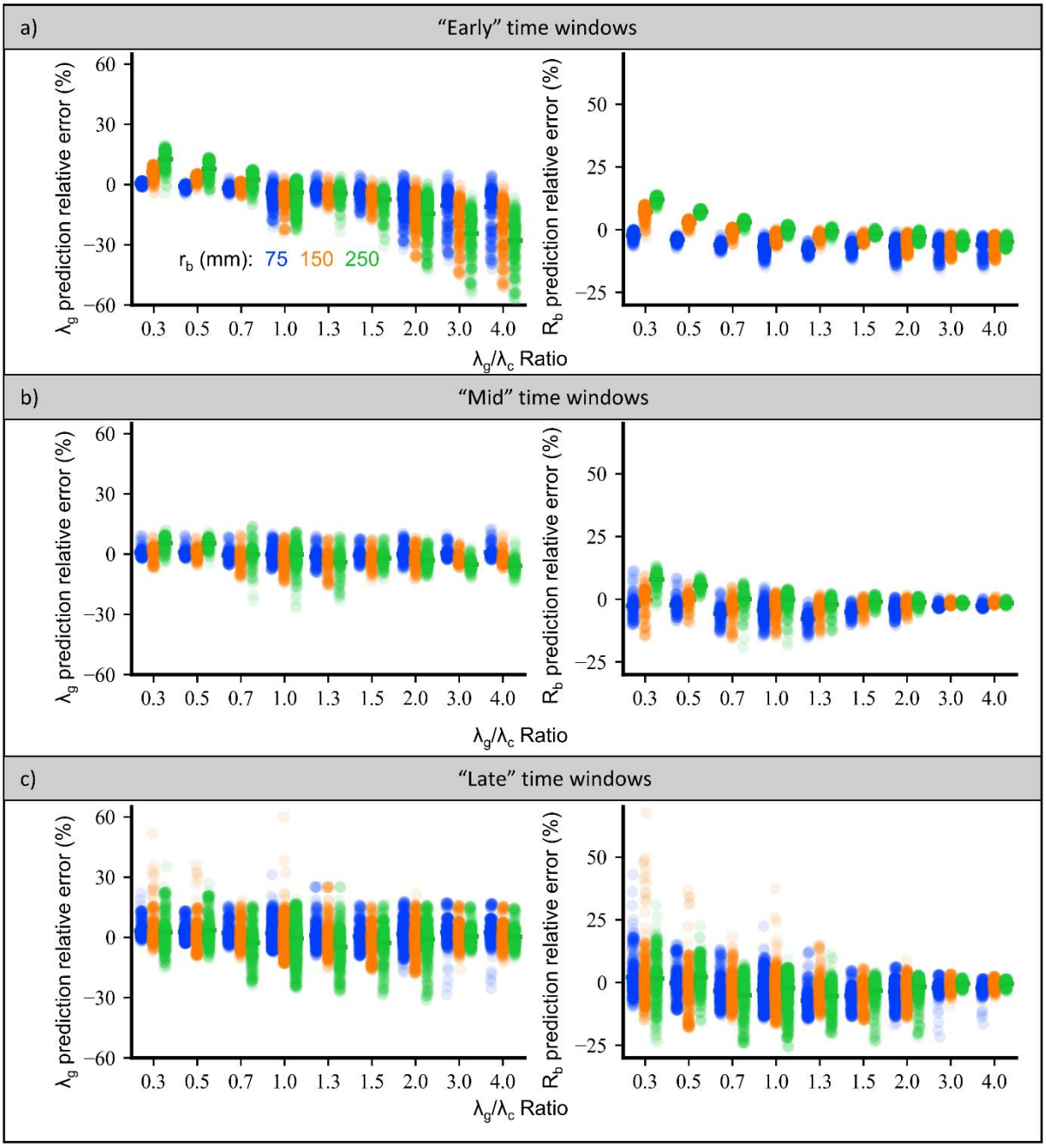

Figure 13 Estimation error of λ_g and R_b obtained for all multiple pile scenarios using the Thermal Interaction approach (ILSM G-functions) with time windows within three distinct time ranges: early (a), mid (b) and late (c).

To further test the proposed Thermal Interference approach for TRT interpretation, the Pile G-functions upper (PGUB) and lower (PGLB) boundary equations are used to obtain the diagonal $G_{i,j}$ components of the **G** matrix (for $i = j$), while the ILSM G-functions are used only for the off-diagonal components (for $i \neq j$). Figure 14 presents the estimation errors obtained for the same time windows as Figure 13 but using the above functions. It can be seen that, overall, the test interpretation using the PGLB results in a larger estimation error range than both PGUB and ILSM G-functions (Figure 13). Moreover, the

performance of the algorithm with the PGLB is particularly inferior for lower λ_g/λ_c ratio values, which likely occurs because the PGLB are better suited for scenarios where λ_g/λ_c ratio is higher than one (Loveridge and Powrie 2013). In addition, low λ_g values result in higher values of time for the same *Fo* number, which suggests that longer time steps are required for calculating the thermal interference when PGLB are used (as stated in Section 3.3), jeopardizing the precision of the results. On the other hand, the estimations using PGUB produce lower error values and lower variance for both λ_g and R_b, especially for early time windows; however, the error value range is still larger than when only the ILSM G-functions are used. Therefore, the use of PGUB functions within the Thermal Interaction approach may be more precise if the group TRT is shorter, while the use of the PGLB functions is mostly unsuitable. A more detailed analysis is required to observe in which scenario the use of the ILSM or the Pile G-functions might be more suitable than the other.

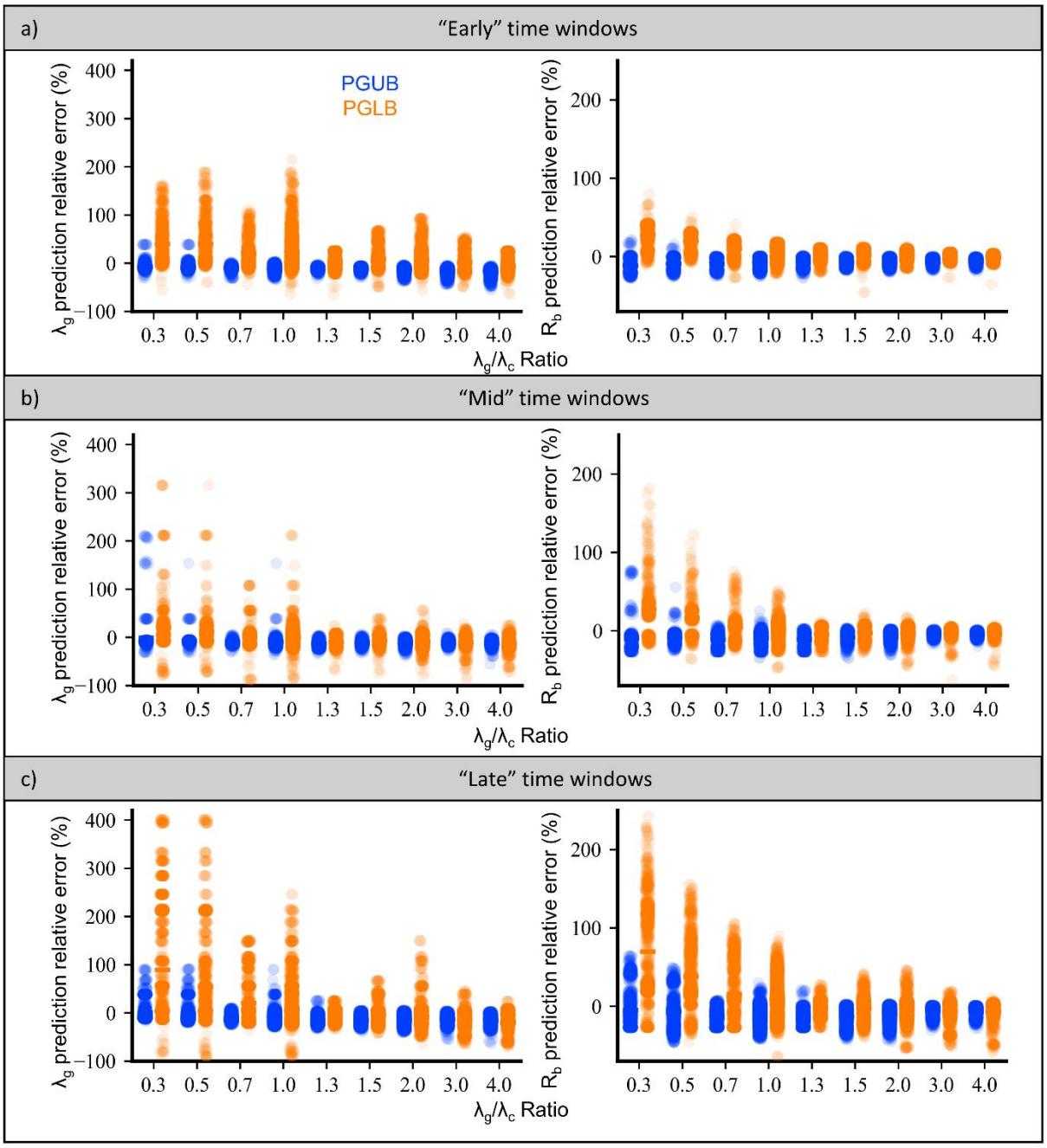

Figure 14 Estimation error of λ_g and R_b obtained for all multiple pile scenarios using the Thermal Interaction approach (Pile G-functions) with time windows within three distinct time ranges: early (a), mid (b) and late (c).

When considering which approach to use for analysing group TRTs, a universal rule to achieve the very best estimation for each one of the numerous scenarios could not be identified within this work. Even though more than 95% of the estimations presented an RMSE equal or lower than 0.1 °C, the range of errors for both estimated parameters λ_g and R_b is significantly large (Appendix C). Nevertheless, the lessons learned from these analyses provide directives to guide the interpretation procedure of group TRTs with significant inter-pile thermal interference, and the "best" results (i.e. lowest errors within a

describable pattern) observed is presented as follows: Firstly, the use of the Thermal Interference approach with the ILSM G-functions populating the entirety of the G-matrix results in estimation errors lower than 5% for both λ_g and R_b for most of the examined scenarios (Figure 15), including considering different time windows for each scenario. The results suggest that the interpretation of R_b can be suitably done considering only early test hours (e.g. 12 to 48 hours), regardless of the pile group configuration and thermal properties. On the other hand, when computing λ_g, different time windows are found to be appropriate fir different scenarios. The traditional $Fo = 5$ threshold used for single pile or BHE elements did not prove to be effective for group TRT interpretation since it does not take into consideration λ_c and it results in a longer test duration that can jeopardize the estimation precision. The suggested interpretation windows for λ_g can be seen in Figure 15b, depending on the values of λ_c and r_b.

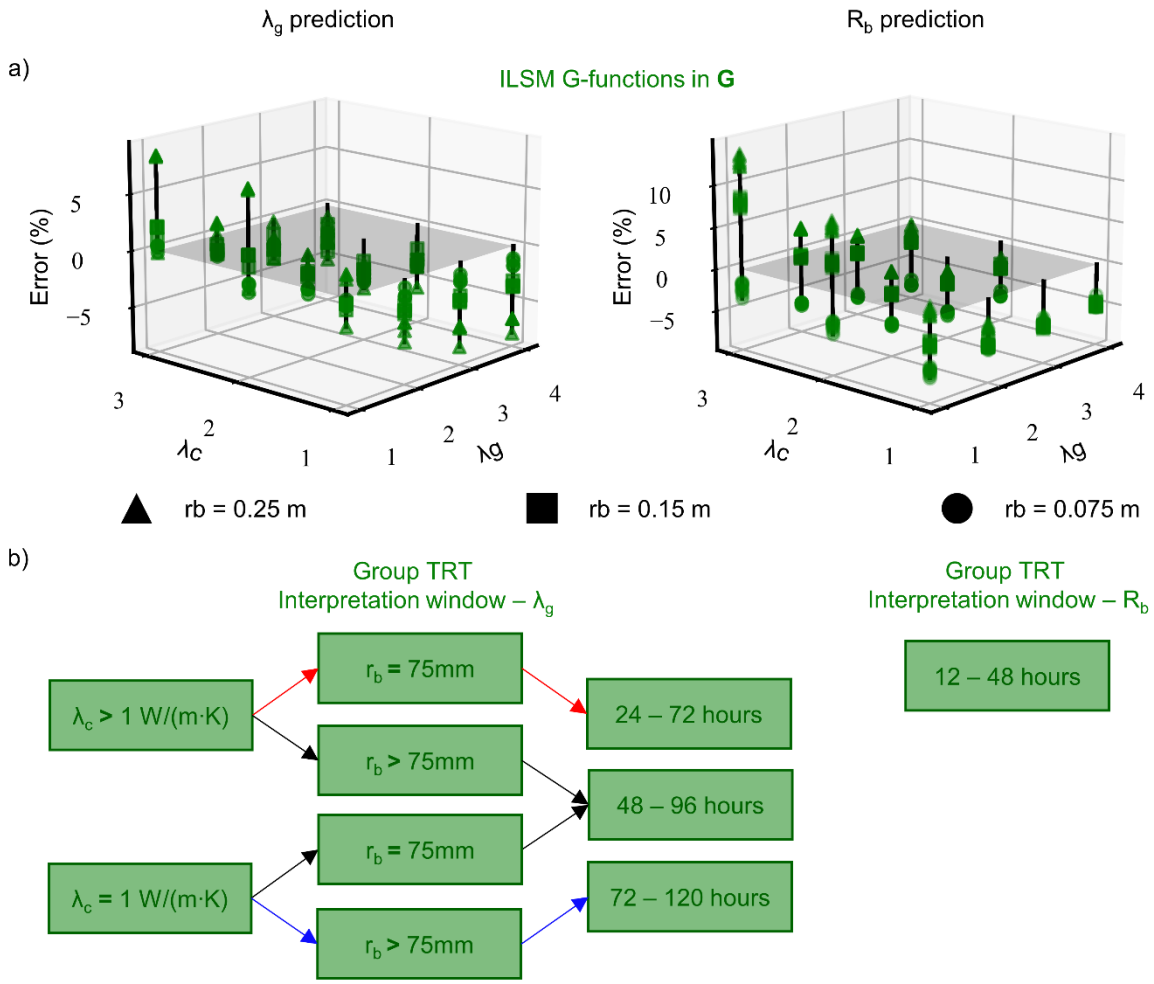

Figure 15. Estimation Error values for both λ_g and R_b (left and right respectively) using the thermal interference approach and ILSM G-functions (a), considering the time windows defined in (b).

Similarly to Figure 15, Figure 16 presents the estimation errors obtained using the Pile G-functions when calculating the individual pile response in the Thermal Interference approach (panel a) for certain time windows (panel b) and disregarding the scenarios with r_b = 75 mm. The time windows selected are from earlier stages in comparison to Figure 15b) because the consideration of transient phase by the Pile G-functions favours precise parameter estimation with earlier test stages. However, most of the errors are higher. For PGLB, the reasons for this are mentioned in this section. In addition, using PGUB produces larger errors when r_b < 250 mm, which indicates that the use of the Pile G-functions in this methodology is more efficient for larger diameter piles (hence, the results for r_b = 75 mm are not presented in Figure 16). Despite the breadth of the errors, the use of the PGUB and the PGLB results in underestimations and overestimations respectively, suggesting that their estimation could be used as upper and lower boundaries by geothermal design engineers.

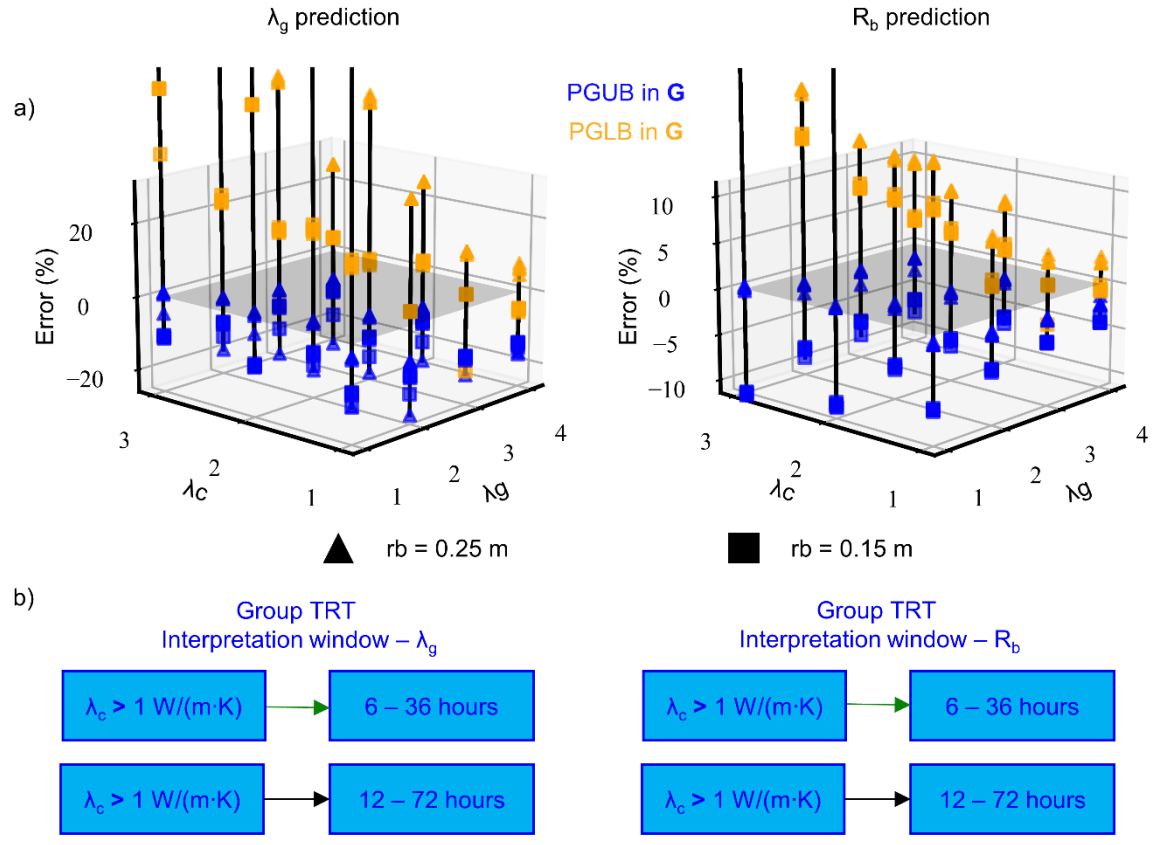

Figure 16. Estimation Error values for both λ_g and R_b (left and right respectively) using the thermal interference approach and Pile specific G-functions (a), considering the time windows defined in (b).

To the best of the authors knowledge, there are no other studies on the interpretation of group TRTs (piles connected in series). However, the results of this work still can be compared to other studies that

evaluated the interpretation of single element TRTs to summarize the key takeaways, since the Thermal Interaction approach is based on the superposition of effects of the same analytical methods that are used to interpret single TRTs. Table 3 presents statements about other works as well as this one.

Table 3 Summary comparison table of this work's results on group TRTs against previous studies on single pile/BHE TRTs.

Study	Analytical models considered	Key takeaways
(Loveridge et al., 2014)	ILSM and Pile G-functions on a single energy pile	ILSM provides a better fit to test results, but test requires 72 hours. Pile G-functions are more reliable for shorter TRTs.
(Zarrella et al., 2017)	Traditional Approach, ILSM, ICSM and numerical methods on single BHE	The numerical methods provided the best fit to test results, followed by the ILSM. Both methods estimations of λ_g the are similar, while ICSM provides lower λ_g values overall.
(Jensen-Page et al., 2019)	Traditional Approach, ILSM, ICSM, FLSM and Pile G-functions on a single Energy Pile	Estimations from the ILSM, FLSM and Pile G-functions are similar and close to the correct values, followed by the Traditional Approach while ICSM is significantly off. Pile G-functions results converge earlier to the correct values.
This work	Traditional Approach and Thermal Interference approach (ILSM, ICSM, FLSM and Pile G-functions) on groups of Energy Piles	The traditional approach estimation errors are high (up to 80% for λ_g and 1000% for Rb) for group tests affected by thermal interference. The Thermal Interference approach lowers these errors to values similar to the other studies on single pile/BHE. The implementation of the ILSM in the Thermal Interference approach provides the lowest errors if the test is no longer than 120 hrs (conditions applied). The Pile G-functions are less suitable for the Thermal Interference approach for scenarios with low λ_g.

5 Summary and Conclusions

This work addresses the thermal behaviour of energy piles during group TRTs and the respective test interpretation. A parametric analysis consisting of 468 scenarios is undertaken to evaluate the influence of thermal properties of both concrete and soil, pile diameter, pile length, number of piles, and the spacing between them on the pile-to-pile thermal interference and consequences on interpreting group TRTs. An analytical methodology that considers pile-to-pile thermal interference, based on the work of Marcotte and Pasquier (2014) is presented and implemented in a dual objective curve fitting algorithm to interpret group TRTs. The algorithm performance is assessed under a broad range of conditions to inform better practices on interpreting group TRTs. The main takeaways from this work include:

- The parametric analysis show that the pile-to-pile thermal interference is higher for scenarios with closely spaced piles and higher values of λg, λc and rb. Scenarios with pile spacing ≥ 5 metres do not present significant thermal interference despite of other parameters.
- In this work, the interpretation of the Group TRTs using the *Traditional approach* (i.e. approximated by a single equivalent-long heat exchanger) provided similar performance to the single BHE cases when the pile-to-pile thermal interference is not significant. However, if there is thermal interference, λ_g is underestimated and R_b is overestimated which may lead to inefficient geothermal design. Pile groups can exchange up to 72.6% less thermal power with the ground in comparison to a BHE with same total length.
- The *Thermal Interaction approach* significantly improves accuracy of thermal parameter estimations. Utilising the ILSM G-functions renders the best results, however the selection of the time window does not strictly follow the same guidelines as for single BHE TRTs. Longer tests may jeopardize group TRT precision, and the optimal test duration is impacted by both λ_c and λ_g, thus *Fo* cannot be solely relied upon since it is derived only from λ_g (Eq. A.3).
- The use of the thermal interference methodology with the Pile G-functions from Loveridge and Powrie (2013) provided good agreement on validation, but with higher errors than using the ILSM. The use of the Pile G-functions is affected by its reasonable approximation to zero on small time steps (specially PGLB), because of the stepwise characteristic of the Thermal

Interference approach. Regardless, PGUB presented reasonable performance specially for larger piles (r_b = 250 mm) and shorter tests.

- The thermal soil conductivity may vary with depth (Cui & Zhou, 2022), which would impact the TRT result and the behaviour of different energy structures in the same site (Bandeira Neto et al., 2023; Lee, 2011; Raymond & Lamarche, 2013). The approaches presented here do not consider these effects, as it is usually done in practice (Franco & Conti, 2020).
- The effect of groundwater flow on single BHE TRTs is usually considered within the resulting soil *effective* thermal conductivity. However, the way that groundwater flow may affect group TRTs is different than single element ones because of thermal plumes. Since this work does not consider this effect, the use of the Thermal Interference approach on group TRTs under influence of significant groundwater flow is yet to be evaluated.
- There are other potential sources of error on the group TRT that are not assessed on the simulated tests, such as ambient temperature, variable thermal power input, and others. However, strategies from TRT literature can be combined with the ones here presented to address those (Abdelaziz, et al., 2015; R. Beier & Smith, 2003; Murphy et al., 2014).

6 CRediT authorship contribution statement

Luis Bandeira Neto: Conceptualisation; Data curation; Methodology; Software; Writing – original draft. **Guillermo Narsilio**: Supervision; Fund acquisition; Writing – review and editing. **Nikolas Makasis**: Conceptualisation; Supervision; Writing – review and editing.

7 Declaration of Competing Interest

The authors declare that they have no known competing financial interests or personal relationships that could have appeared to influence the work reported in this paper.

8 Acknowledgments

This work was funded by the Australian Research Council (project number LP160101486) and the University of Melbourne. Support from The University of Melbourne's Research Computing Services and the Petascale Campus Initiative Assistance in the computational analysis is much appreciated. This research was supported by use of the Nectar Research Cloud, a collaborative Australian research

653 platform supported by the NCRIS-funded Australian Research Data Commons (ARDC). The first
654 author acknowledges the support from Dr Linden Jensen-Page and Stephan Düber with the Python code
655 used in this work.

656

9 Appendix A: Analytical models

This section describes the analytical models' equations that were considered in this work. Firstly, the **ILSM** equation is presented below:

$$T(t) = T_0 + qR_b + q \cdot \overbrace{\frac{1}{4\pi\lambda_g} \int_{\frac{r_b^2}{4\alpha_g t}}^{\infty} \frac{e^{-u}}{u} du}^{G_{ILSM}} \tag{A.1}$$

where T(t) is the (infinite line) temperature evolution (°C) over time t (s), T_0 is the undisturbed ground temperature (°C), q is the heat energy inserted per metre length of the BHE (W/m), r_b is the BHE radius (m), α_g is the ground thermal diffusivity (m^2/s). When q is constant over time (i.e., TRT), the relationship between T(t) and the logarithm of t is linear after a certain period of time. This log-linear form of the ILSM Eq. (A.1) can be simplified as Eq. (A.2) to obtain the λ_g value from the TRT. Following the same principle, R_b can be obtained from Eq. (A.4) (Beier & Smith, 2002).

$$\lambda_g = \frac{q}{4\pi m} \tag{A.2}$$

$$Fo = \frac{\alpha_g t}{r_b^2} \tag{A.3}$$

$$R_b = \frac{1}{4\pi\lambda_g}\left[\frac{\mathrm{T}(t_{1sec}) - T_0}{m} - \ln\left(\frac{4\alpha_g t_1}{e^{\gamma} r_b^2}\right)\right] \tag{A.4}$$

where m is the slope of the line obtained by plotting the average fluid temperature from the TRT test against the natural logarithm of time (base e), *Fo* is the Fourier number, $T(t_{1sec})$ is the intercept in the *ln* space and γ is the Euler constant. According to Hellstrom (1992), Eq. (A.2) is valid for $Fo \geq 5$.

The Infinite Cylindrical Source Model (**ICSM**) (Ingersoll et al., 1954) (Eq. (5)) presents a more complex solution, where it is not possible to isolate λ_g and R_b such as done with the ILSM.

$$T(Fo, p) = T_0 + \frac{Q}{H} R_b + q \cdot \overbrace{\frac{1}{\pi^2 \lambda_g} \int_0^{\infty} \frac{e^{-u^2 Fo} - 1}{J_1^2(u) + Y_1^2(u)} [J_0(pu)Y_1(u) - J_1(u)Y_0(pu)] \frac{du}{u^2}}^{G_{ICSM}} \tag{A.5}$$

where p = r/rb and r is the radial coordinate, J_0, and J_1 are Bessel functions of the first kind and Y_0 and Y_1 are Bessel functions of the second kind.

675 The first solution of the finite linear source model (**FLSM**) (Eq. (A.6)) was proposed by Claesson and
676 Eskilson (1988). For simplicity, the use of the temperature at mid-depth = H/2 as an average of the
677 whole BHE is recommended. Later, Zeng et al. (2002) showed that this assumption overestimates the
678 borehole temperature and proposed a solution of an integral average of the whole BHE. This solution
679 was later simplified by Lamarche and Beauchamp (2007a) (Eqs. (7) to (11)).

$$T(t,r,z) = T_0 + \frac{Q}{H}R_b + q \cdot \overbrace{\frac{1}{4\pi\lambda_g}\int_0^H \left[\frac{erfc\left(\frac{\sqrt{r^2+(z-s)^2}}{2\sqrt{\alpha_g t}}\right)}{\sqrt{r^2+(z-s)^2}} - \frac{erfc\left(\frac{\sqrt{r^2+(z+s)^2}}{2\sqrt{\alpha_g t}}\right)}{\sqrt{r^2+(z+s)^2}}\right] ds}^{G_{FLSM}} \quad \text{(A.6)}$$

$$T(t,\beta) = T_0 + \frac{Q}{H}R_b + q \cdot \overbrace{\frac{1}{2\pi\lambda_g}\left[\int_\beta^{\sqrt{\beta^2+1}} \frac{erfc(\omega z)}{\sqrt{z^2-\beta^2}} dz - D_A - \int_{\sqrt{\beta^2+1}}^{\sqrt{\beta^2+4}} \frac{erfc(\omega z)}{\sqrt{z^2-\beta^2}} dz - D_B\right]}^{G_{FLSM-Lamarche}} \quad \text{(A.7)}$$

$$D_A = \sqrt{\beta^2+1}\cdot erfc\left(\omega\sqrt{\beta^2+1}\right) - \beta erfc(\omega\beta) - \frac{e^{-\omega^2(\beta^2+1)} - e^{-\omega^2\beta^2}}{\beta\sqrt{\pi}} \quad \text{(A.8)}$$

$$D_B = \sqrt{\beta^2+1}\cdot erfc\left(\omega\sqrt{\beta^2+1}\right) - 0.5\left(\beta erfc(\omega\beta) + \sqrt{\beta^2+4}\cdot erfc\left(\omega\sqrt{\beta^2+4}\right)\right) - \frac{e^{-\omega^2(\beta^2+1)} - 0.5\left(e^{-\omega^2\beta^2} + e^{-\omega^2(\beta^2+4)}\right)}{\beta\sqrt{\pi}} \quad \text{(A.9)}$$

$$\omega = \frac{1}{2\beta\sqrt{Fo}} \qquad \beta = \frac{r_b}{H} \quad \text{(A.10)} \quad \text{(A.12)}$$

680

681 where z is the borehole depth where the temperature is calculated (m), r is the radial coordinate
682 (m), and *erfc* is the complimentary error function.

683

684

10 Appendix B: Numerical model governing equations

The numerical model approach used in this work coupled governing equations of heat transfer and fluid flow. Fluid flow modelling is based on the momentum and continuity equations (Eqs. B.1 and B.2 respectively), considering that the fluid is incompressible. The heat transfer within the heat carrier fluid considers both conduction and convection (Eq. B.3 and Eq. B.4) while all other materials consider heat conduction only (Eq. B.5).

$$A\rho_f \nabla \cdot \boldsymbol{v} = 0$$

$$\rho_f \left(\frac{\partial \boldsymbol{v}}{\partial t}\right) = -\nabla p - f_D \frac{\rho_f}{2d_h} \boldsymbol{v}|\boldsymbol{v}| \quad \text{(B.1)}$$

$$\rho_f A C_{p,f} \frac{\partial T_f}{\partial t} + \rho_f A C_{p,f} \boldsymbol{v} \cdot \nabla T_f = \nabla \cdot \left(A \lambda_f \nabla T_f\right) + f_D \frac{\rho_f A}{2d_h} |\boldsymbol{v}|\boldsymbol{v}^2 + Q_{wall} \quad \text{(B.2)}$$

$$Q_{wall} = f\left(T_{pipe\ wall}, T_f, \lambda_p, d_p\right) \quad \text{(B.3)}$$

$$\rho_m C_{p,m} \frac{\partial T_m}{\partial t} = \nabla \cdot (\lambda_m \nabla T_m) \quad \text{(B.4)}$$

where A is the inner cross-section of the HDPE pipes, ρ_w is the carrier fluid density, v is the fluid velocity vector field, t is the time, p is the pressure, f_D represents the Darcy friction factor, d_h is the hydraulic diameter of the pipe. $C_{p,f}$ represents the fluid's specific heat capacity, λ_f is the fluid thermal conductivity. Q_{wall} stands for the external heat exchange rate through the pipe wall, which is a function of the temperature on the pipe outer wall ($T_{pipe\ wall}$), the fluid temperature (T_f), the pipe wall thermal conductivity and the pipe diameter. ρ_m is the material density, $C_{p,m}$ is the material specific heat capacity, T_m is the material temperature field and λ_m is the thermal conductivity of the material.

In all models considered in this work, the inlet fluid temperature was determined from the thermal power Q using the Eq. (B.5):

$$T_{in} = \frac{Q}{\dot{m} C_{p,f}} + T_{out} \quad \text{(B.5)}$$

where T_{in} and T_{out} are the fluid inlet and outlet temperatures respectively, $\dot{m}$ is the mass fluid flow rate and $C_{p,f}$ is the fluid specific heat capacity.

A mesh analysis is conducted for all geometries. Table B.1 presents the mean absolute percentage error (MAPE) of the fluid temperatures obtained by comparing the results of the models considered in this work with simulations executed with denser meshes (i.e. more elements). The increase in the number

of elements is presented as a percentage of the original since the element number is slightly for each geometry. Table B.1 presents the results for each one of the geometries (1, 2, 4 and 8 piles).

Table B.1 Mesh analysis results for all model geometries considered.

Geometry	Fluid temperature MAPE according to model element Nº increase (%)	
	25% increase	50% increase
1 Pile	0.120 %	0.192 %
2 Piles	0.040 %	0.044 %
4 Piles	0.237 %	0.230 %
8 Piles	0.052 %	0.186 %

11 Appendix C: Distribution of the error values

The figure bellow presents the histograms of the final RMSE values and both λ_g and R_b estimation relative errors obtained on ALL group TRT tests presented in this work.

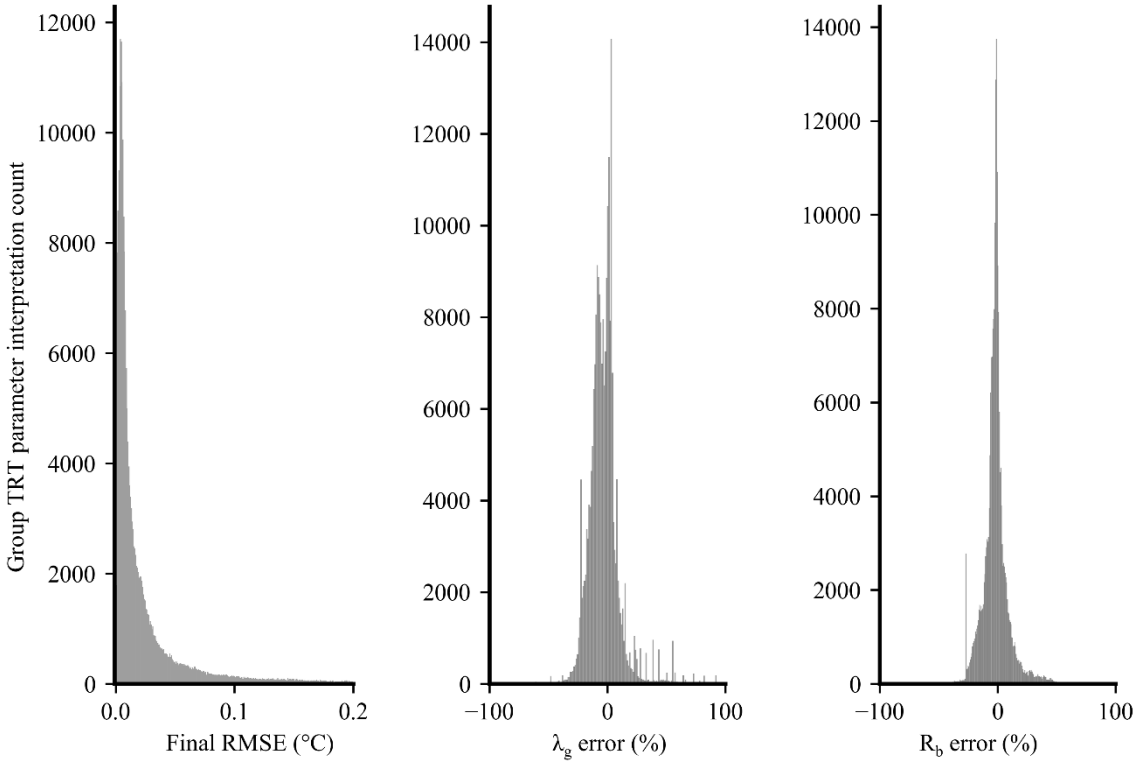

Figure C.1. Histograms of final RMSE (a), λ_g estimation (b) and R_b estimation (c) relative errors from all group TRT estimations executed with the thermal interference methodology.

13 References

Abdelaziz, S. L., Olgun, C. G., & Martin, J. R. (2015). Counterbalancing ambient interference on thermal conductivity tests for energy piles. Geothermics, 56, 45-59. doi:https://doi.org/10.1016/j.geothermics.2015.03.005

Austin III, W. A. (1998). Development of an in situ system for measuring ground thermal properties. Thesis (PhD). Oklahoma State University, Stillwater – Oklahoma, USA.

Bandeira Neto, L., Narsilio, G., Makasis, N., Choudhary, R., & Carden, Y. (2023). Thermal response of energy screw piles connected in series. J. of Geotech. and Geoenv. Eng., in press. https://doi.org/10.1061/JGGEFK/GTENG-11082.

Beier, R., & Smith, M. D. (2003). Removing variable heat rate effects from borehole tests. ASHRAE Transactions, 109, 463-474.

Beier, R. A., & Smith, M. D. (2002). Borehole thermal resistance from line-source model of in-situ tests. ASHRAE Transactions, 108, 212.

Bidarmaghz, A. (2014). 3D numerical modelling of vertical ground heat exchangers. Thesis (PhD) The University of Melbourne, Melbourne, Australia.

Bidarmaghz, A., Makasis, N., Narsilio, G. A., Francisca, F. M., & Carro Pérez, M. E. (2016). Geothermal energy in loess. Env. Geotech., 3(4), 225-236. doi:10.1680/jenge.15.00025

Bouazza, A., Manassero, M., Wang, B., Dominijanni, A., Singh, R. M., Foti, S., Musso, G. (2013). Soil effective thermal conductivity from energy pile thermal tests. Proc. Int. Cong. on Env. Geotech. (ICEG), Torino Italy, Leiden The Netherlands.

Brandl, H. (2006). Energy foundations and other thermo-active ground structures. Géotechnique, 56(2), 81-122. doi:10.1680/geot.2006.56.2.81

Carslaw, H., & Jaeger, J. (1959). Conduction of Heat in Solids (Clarendon, Oxford).

Claesson, J., & Eskilson, P. (1988). Conductive heat extraction to a deep borehole: Thermal analyses and dimensioning rules. Energy, 13(6), 509-527. doi:https://doi.org/10.1016/0360-5442(88)90005-9

744 Colls, S., Narsilio, G. A., & Johnston, I. W. (2012). Experimental study of ground energy systems in
745 Melbourne, Australia. Proc. 11th AUS - NZ Conf. on Geomech., Melbourne - Australia.
746 COMSOL. (2021). COMSOL Multiphysics v. 5.6. COMSOL AB, Stockolm, Sweden.
747 Cui, S. Q., & Zhou, C. (2022). Coupled effects of stress state and void ratio on thermal conductivity of
748 saturated soils. Géotechnique Letters, 12(2), 148-153. https://doi.org/10.1680/jgele.22.00001
749 EklÖF, C., & Gehlin, S. (1996). A Mobile Equipment for Thermal Response Test.
750 Eskilson, P. (1987). Thermal analysis of heat extraction boreholes.
751 Franco, A., & Conti, P. (2020). Clearing a Path for Ground Heat Exchange Systems: A Review on
752 Thermal Response Test (TRT) Methods and a Geotechnical Routine Test for Estimating Soil
753 Thermal Properties. Energies, 13(11), 2965. https://www.mdpi.com/1996-1073/13/11/2965
754 Franco, A., Moffat, R., Toledo, M., & Herrera, P. (2016). Numerical sensitivity analysis of thermal
755 response tests (TRT) in energy piles. Renew. Energy, 86, 985-992.
756 doi:https://doi.org/10.1016/j.renene.2015.09.019
757 Gehlin, S. (2002). Thermal response test : method development and evaluation. Thesis (PhD). Luleå
758 tekniska universitet, Luleå.
759 Hellstrom, G. (1992). Ground heat storage: Thermal analyses of duct storage systems.
760 Ingersoll, L. R., Zabel, O. J., & Ingersoll, A. C. (1954). Heat conduction with engineering, geological,
761 and other applications.
762 Jensen-Page, L., Loveridge, F., & Narsilio, G. A. (2019). Thermal Response Testing of Large Diameter
763 Energy Piles. Energies, 12(14), 2700.
764 Jones, E., Oliphant, T., Peterson, P., & others. (2001). SciPy: Open source scientific tools for Python.
765 Katsura, T., Nagano, K., Narita, S., Takeda, S., Nakamura, Y., & Okamoto, A. (2009). Calculation
766 algorithm of the temperatures for pipe arrangement of multiple ground heat exchangers. Appl.
767 Thermal Eng., 29(5), 906-919. doi:https://doi.org/10.1016/j.applthermaleng.2008.04.026
768 Lamarche, L., & Beauchamp, B. (2007a). A new contribution to the finite line-source model for
769 geothermal boreholes. Energy and Buildings, 39(2), 188-198.
770 doi:https://doi.org/10.1016/j.enbuild.2006.06.003

771 Lamarche, L., & Beauchamp, B. (2007b). New solutions for the short-time analysis of geothermal
772 vertical boreholes. Inte. J. of Heat and Mass Transfer, 50(7), 1408-1419.
773 doi:https://doi.org/10.1016/j.ijheatmasstransfer.2006.09.007
774 Lee, C. K. (2011). Effects of multiple ground layers on thermal response test analysis and ground-
775 source heat pump simulation. Appl. Energy, 88(12), 4405-4410.
776 https://doi.org/https://doi.org/10.1016/j.apenergy.2011.05.023
777 Li, M., & Lai, A. C. K. (2012a). New temperature response functions (G functions) for pile and borehole
778 ground heat exchangers based on composite-medium line-source theory. Energy, 38(1), 255-
779 263. doi:https://doi.org/10.1016/j.energy.2011.12.004
780 Li, M., & Lai, A. C. K. (2012b). Parameter estimation of in-situ thermal response tests for borehole
781 ground heat exchangers. Int. J. of Heat and Mass Transfer, 55(9), 2615-2624.
782 doi:https://doi.org/10.1016/j.ijheatmasstransfer.2011.12.033
783 Li, M., & Lai, A. C. K. (2015). Review of analytical models for heat transfer by vertical ground heat
784 exchangers (GHEs): A perspective of time and space scales. Appl. Energy, 151, 178-191.
785 doi:https://doi.org/10.1016/j.apenergy.2015.04.070
786 Li, Z., Wang, C., & Fu, Q. (2022). Effects of groundwater flow on thermal response test of deep
787 borehole heat exchanger. Geothermics, 106, 102570.
788 https://doi.org/https://doi.org/10.1016/j.geothermics.2022.102570
789 Loveridge, F., McCartney, J. S., Narsilio, G. A., & Sanchez, M. (2020). Energy geostructures: A review
790 of analysis approaches, in situ testing and model scale experiments. Geomech. for Energy and
791 the Env., 22, 100173. doi:https://doi.org/10.1016/j.gete.2019.100173
792 Loveridge, F., Olgun, C., Brettmann, T., & Powrie., W. (2015). Group thermal response testing for
793 energy piles. In Geotech. Eng. for Infrastructure and Development (pp. 2595-2600).
794 Loveridge, F., & Powrie, W. (2013). Temperature response functions (G-functions) for single pile heat
795 exchangers. Energy, 57, 554-564. doi:https://doi.org/10.1016/j.energy.2013.04.060
796 Loveridge, F., & Powrie, W. (2014a). 2D thermal resistance of pile heat exchangers. Geothermics, 50,
797 122-135. doi:https://doi.org/10.1016/j.geothermics.2013.09.015

798 Loveridge, F., & Powrie, W. (2014b). G-Functions for multiple interacting pile heat exchangers.
799 Energy, 64, 747-757. doi:https://doi.org/10.1016/j.energy.2013.11.014
800 Loveridge, F., Powrie, W., & Nicholson, D. (2014). Comparison of two different models for pile
801 thermal response test interpretation. Acta Geotechnica, 9(3), 367-384. doi:10.1007/s11440-
802 014-0306-3
803 Lu, Q., & Narsilio, G. A. (2019). Cost effectiveness of energy piles in residential dwellings in Australia.
804 Cur Trends Civil & Struct Eng. 3(3). CTCSE.MS.ID.000564.
805 Magraner, T., Montero, Á., Cazorla-Marín, A., Montagud-Montalvá, C., & Martos, J. (2021). Thermal
806 response test analysis for U-pipe vertical borehole heat exchangers under groundwater flow
807 conditions. Renew. Energy, 165, 391-404.
808 https://doi.org/https://doi.org/10.1016/j.renene.2020.11.029
809 Makasis, N. (2019). Further understanding ground source heat pump system design using finite element
810 methods and machine learning techniques. Thesis (PhD) The University of Melbourne,
811 Melbourne, Australia.
812 Makasis, N., Narsilio, G. A., & Bidarmaghz, A. (2018). A robust prediction model approach to energy
813 geo-structure design. Comp. and Geotech., 104, 140-151. doi:10.1016/j.compgeo.2018.08.012
814 Makasis, N., Narsilio, G. A., Bidarmaghz, A., & Johnston, I. W. (2018). Ground-source heat pump
815 systems: The effect of variable pipe separation in ground heat exchangers. Comp. and Geotech.,
816 100, 97-109. doi:https://doi.org/10.1016/j.compgeo.2018.02.010
817 Man, Y., Yang, H., Diao, N., Liu, J., & Fang, Z. (2010). A new model and analytical solutions for
818 borehole and pile ground heat exchangers. Int. J. of Heat and Mass Transfer, 53(13), 2593-
819 2601. doi:https://doi.org/10.1016/j.ijheatmasstransfer.2010.03.001
820 Marcotte, D., & Pasquier, P. (2008). On the estimation of thermal resistance in borehole thermal
821 conductivity test. Renew. Energy, 33(11), 2407-2415.
822 doi:https://doi.org/10.1016/j.renene.2008.01.021
823 Marcotte, D., & Pasquier, P. (2014). Unit-response function for ground heat exchanger with parallel,
824 series or mixed borehole arrangement. Renew. Energy, 68, 14-24.
825 doi:https://doi.org/10.1016/j.renene.2014.01.023

826 Mogensen, P. K. (1983). Fluid to duct wall heat transfer in duct system heat storages.
827 Morais, T. d. S. O., Tsuha, C. d. H. C., Bandeira Neto, L. A., & Singh, R. M. (2020). Effects of seasonal
828 variations on the thermal response of energy piles in an unsaturated Brazilian tropical soil.
829 Energy and Buildings, 216, 109971. doi:https://doi.org/10.1016/j.enbuild.2020.109971
830 Motamedi, Y., Makasis, N., Gu, X., Narsilio, G. A., Arulrajah, A., & Horpibulsuk, S. (2021).
831 Investigating the thermal behaviour of geothermal pavements using Thermal Response Test
832 (TRT). Transp. Geotech., 29, 100576. doi:https://doi.org/10.1016/j.trgeo.2021.100576
833 Murphy, K. D., McCartney, J. S., & Henry, K. S. (2014). Impact of Horizontal Run-Out Length on the
834 Thermal Response of Full-Scale Energy Foundations. In Geo-Cong. 2014 Tech. Papers (pp.
835 2715-2724).
836 Narsilio, G. A., & Aye, L. (2018). Shallow Geothermal Energy: An Emerging Technology. In A.
837 Sharma, A. Shukla, & L. Aye (Eds.), Low Carbon Energy Supply: Trends, Technology,
838 Management (pp. 387-411). Singapore: Springer Singapore.
839 Pasquier, P., & Marcotte, D. (2013). Efficient computation of heat flux signals to ensure the
840 reproduction of prescribed temperatures at several interacting heat sources. Appl. Thermal
841 Engineering, 59(1), 515-526. doi:https://doi.org/10.1016/j.applthermaleng.2013.06.018
842 Philippe, M., Bernier, M., & Marchio, D. (2009). Validity ranges of three analytical solutions to heat
843 transfer in the vicinity of single boreholes. Geothermics, 38(4), 407-413.
844 doi:https://doi.org/10.1016/j.geothermics.2009.07.002
845 Raymond, J., & Lamarche, L. (2013). Simulation of thermal response tests in a layered subsurface.
846 Appl. Energy, 109, 293-301. https://doi.org/https://doi.org/10.1016/j.apenergy.2013.01.033
847 Wood, C., Liu, H., & Riffat, S. (2010). Comparison of a modelled and field tested piled ground heat
848 exchanger system for a residential building and the simulated effect of assisted ground heat
849 recharge. Int. J. of Low-Carbon Tech., 5, 137-143. doi:10.1093/ijlct/ctq015
850 Yu, X., Zhang, Y., Deng, N., Wang, J., Zhang, D., & Wang, J. (2013). Thermal response test and
851 numerical analysis based on two models for ground-source heat pump system. Energy and
852 Buildings, 66, 657-666. doi:https://doi.org/10.1016/j.enbuild.2013.07.074

Zarrella, A., Emmi, G., Graci, S., De Carli, M., Cultrera, M., Santa, G. D., Galgaro, A., Bertermann, D., Müller, J., Pockelé, L., Mezzasalma, G., Righini, D., Psyk, M., & Bernardi, A. (2017). Thermal Response Testing Results of Different Types of Borehole Heat Exchangers: An Analysis and Comparison of Interpretation Methods. Energies, 10(6), 801. https://www.mdpi.com/1996-1073/10/6/801

Zeng, H. Y., Diao, N. R., & Fang, Z. H. (2002). A finite line-source model for boreholes in geothermal heat exchangers. Heat Transfer—Asian Research, 31(7), 558-567. doi:https://doi.org/10.1002/htj.10057

Zeng, S., Yan, Z., & Yang, J. (2022). Stepwise algorithm and new analytical model for estimating multi-parameter of energy piles from thermal response tests. Energy and Buildings, 256, 111775. doi:https://doi.org/10.1016/j.enbuild.2021.111775

Zhang, X., Zhang, T., Li, B., & Jiang, Y. (2019). Comparison of Four Methods for Borehole Heat Exchanger Sizing Subject to Thermal Response Test Parameter Estimation. Energies, 12, 4067. doi:10.3390/en12214067

Zhong, Y., Narsilio, G. A., Makasis, N., & Scott, C. (2022). Experimental and numerical studies on an energy piled wall: The effect of thermally activated pile spacing. Geomech. for Energy and the Env., 29, 100276. doi:https://doi.org/10.1016/j.gete.2021.100276

List of Figures

List of Tables